THERMAL EFFUSION STUDIES ON POROUS SILICON

by

JITENDRA SINGH

Th
MSP/1997/14
Si 64 t



MATERIALS SCIENCE PROGRAMME

INDIAN INSTITUTE OF TECHNOLOGY KANPUR

FEBRUARY 1997

THERMAL EFFUSION STUDIES ON POROUS SILICON

A Thesis Submitted in
Partial Fulfilment of the Requirements
for the Degree of
MASTER OF TECHNOLOGY

by
JITENDRA SINGH

to the
Material Science Programme
Indian Institute of Technology, Kanpur
February 1997

19 MAR 97
CENTRAL LIBRARY
Acc. No. A 123253

CERTIFICATE

This is to certify that the present work entitled **Thermal Effusion Studie on Porous Silicon** *has been carried out by* **Jitendra Singh** *under our supervisio and it has not been submitted elsewhere for a degree to the best of our knowledge.*

S Kumar 24/2/97

Dr. Satyendra Kumar
Department of Physics
Indian Institute of Technology
Kanpur

Y N Mohapatra

Dr. Y.N. Mohapatra
Department of Physics &
Material Science Programme
Indian Institute of Technology
Kanpur



Febuary 1997

Abstract

The observation of room temperature visible photoluminescence from porous silicon has recently stimulated considerable research from both fundamental and technological points of view. One of the least studies aspects of these material, however, is its thermal stability and the role and nature of chemical species present in the large surface area of the material. With large internal surfaces, the chemicals present on them are likely to have large influence on its properties.

Room temperature photoluminescent porous silicon samples have been prepared and characterized using a variety of techniques such as infrared, Raman, photoluminescence and thermally stimulated effusion spectroscopies. In particular, thermally stimulated effusion spectra of effusing species have been analysed in detail to understand the nature of hydrogen bonding and its thermal release from porous silicon. Microstructural information obtained from Raman and infrared spectra have been correlated with the results of thermal effusion studies. Photoluminescence spectroscopy of these samples show a broad peak at around 1.8 eV with a FWHM of about 350 meV. A large number of ionic species were identified in the thermal effusion spectra of PS samples. Significant among them are the hydrides and fluorides of silicon. In addition, residual carbonic species along with moisture were detected. The thermally stimulated spectra of individual ions from room temperature to 800°C were analyzed as a function varying heating rates. Molecular hydrogen effusion shows two major peaks about 400 and about 500°C. The low temperature peak is attributed to hydrogen desorption from SiH_2 and the high temperature to that from SiH. Micro-Raman studies on as prepared samples reveal presence of silicon nano-crystallites of size 3-4 nm. The presence of Raman shifts at about 480 cm^{-1} clearly indicate existence of amorphous silicon in the sample. Raman spectra shows that on heating the sample in the range of 500 to 760°C, there is decrease in the size of the nanocrystallite and increase in the disordered component. Infrared spectra of as prepared samples show sharp spectral features around 2100 cm^{-1} due to stretching modes of hydrides of silicon indicating well defined hydrogen chemisorption sites in porous silicon. The observation of photoluminescence, even after heat treatment at 495°C, has been attributed to surface passivation of defects due to oxidation.

ACKNOWLEDGEMENTS

I am extremely thankful to my thesis supervisors Dr. Satyendra Kumar and Dr. Y.N. Mohapatra for being extremely cooperative and understanding throughout my M.Tech thesis. They have taught me many things and helped me in many ways, in both academic and other matters.

I would like to thank in particular Ms. Manju Malhotra for helping me in carrying out my experiments on thermal effusion in our laboratory. I am also thankful to N. Islam for preparing electrochemical cell, Dr. Jitendra Kumar and Rajesh Kumar for Al deposition on Si-wafers, Dr. V.N. Kulkarni and Rajneesh Kumar Gupta for thermal annealing for Al deposited Si-wafers, Dr. Asima Pradhan and Dr. P.K. Khulbe for Raman and photoluminescence measurements, and Dr. Rambilas and Rajender Kumar for technical help.

Jitendra Singh

Contents

List of Figures viii

1 Introduction 1

1.1 Etching of Si-Surface . . . 3

1.1.1 Electrochemical Etching . . . 3

1.1.2 Photochemical Etching . . . 3

1.1.3 Chemical Etching . . . 4

1.1.4 Spark Erosion Technique . . . 4

1.2 Porous Silicon Formation Mechanisms . . . 4

1.3 Luminescence Behaviour . . . 5

1.3.1 Photoluminescence . . . 6

1.3.2 Electroluminescence . . . 7

1.3.3 Electrochemiluminescence . . . 8

1.4 Vibrational Spectroscopy . . . 8

1.4.1 Raman Spectroscopy . . . 9

1.4.2 Infrared Spectroscopy . . . 10

1.5 Statement of the Problem . . . 11

2 Experimental 13

2.1 Sample Preparation 13
2.1.1 Si-Wafer Cleaning 13
2.1.2 Al-Deposition on Si-wafer 14
2.1.3 Thermal Annealing of Al-deposited Si-wafer 14
2.1.4 Electrochemical Etching of Si-Wafer 17
2.1.5 Drying Process of Fresh Porous Silicon Sample 17
2.2 Mass Spectroscopic Thermal Effusion Set-up 19
2.2.1 Quartz Tube with a Furnace 19
2.2.2 Quadrupole Gas Analyzer 22
2.2.3 Calibration of Temperature 22
2.3 Characterization of Porous Silicon Sample 24
2.3.1 Mass Spectroscopic Thermal Effusion 24
2.3.2 Raman Spectroscopy and Photoluminescence Measurements . 24
2.3.3 Infrared Spectroscopy 25
2.4 Peakfit Analysis 25

3 Results and Discussion **27**

3.1 Photoluminescence from Porous Silicon 27
3.2 Mass Spectroscopic Thermal Effusion 30
3.2.1 General Behaviour 32
3.2.2 Thermally Stimulated Desorption Kinetics 36
3.3 Desorption of Hydrogen 39
3.3.1 Effect of Heating Rate on Hydrogen Desorption 39
3.3.2 PSL Thickness Effect on Hydrogen Desorption 49
3.4 Raman Analysis 52
3.5 IR Analysis 56

4 Summary and Conclusions 61

Bibliography 64

List of Figures

1.1 pn-heterojunction fabricated by using porous silicon layer 7

1.2 Stokes Raman and anti-Stokes Raman effects 10

2.1 Schematic diagram of Al-deposition set-up 15

2.2 Schematic diagram of annealing set-up 16

2.3 Schematic diagram of teflon cell 18

2.4 Porous-Si Sample 19

2.5 Schematic diagram of Mass Spectroscopic Thermal Effusion Set-up DPM : Differential Penning Meter(for temperature measurement), RGA : Residual Gas Analyzer, DPM : Differential Pressure Units, QGA : Quadruple Gas Analyzer, PC : Personnel Computer 20

2.6 Schematic diagram of heating tube with furnace 21

2.7 Typical heating rates used in thermal effusion PS samples 23

2.8 A typical peakfit analysis for hydrogen peaks. 26

3.1 Photoluminescence spectra from 20 min porous silicon sample. (a) unheated. (b) heated upto 495°C/min with heating rate 6.2°C/min. (c) heated upto 760°C with heating rate 18°C/min. 29

3.2 Mass spectra of thermal desorption from porous silicon. The peaks are centralized around m/e 2, 15, 30, 42, 55, 70, and 82 with some other small peaks 31

3.3 Effusion curve for thermal desorption from 20 min sample (PS2) heated at the rate of 16°C/min. The clear peaks for hydrides of silicon appear at 360°C. Hydrogen peaks are at 396°C and 496°C. 34

3.4 Effusion curve for thermal desorption of CH_3. It is found to decrease continuously as the temperature increases. 35

3.5 Effusion curve for thermal desorption of SiH_4. It is also found to decrease continuously as the temperature increases. 35

3.6 Hydrogen effusion curves for thermal desorption from porous silicon . 40

3.7 Hydrogen peaks shift as heating rate is changed for 10 min sample (PS1) 42

3.8 Arrhenious plots for 10 min sample (PS1) 43

3.9 (a) H_2 and (b) SiH_3 semi-logarithmic effusion curves for thermal desorption from porous silicon as temperature is increased for 10 min sample (PS1) 46

3.10 Effusion curves for thermal desorption from porous silicon for different heating rates of 10 min sample (a) Heating rate 18°C/min (b) Heating rate 36°C/min (c) Heating rate 62°C/min 47

3.11 Hydrogen effusion curves for thermal desorption from porous silicon as the etching time for sample preparation is changed. 50

3.12 Raman spectra of porous silicon samples (a) Standard c-Si (b) 20 min sample, as-prepared (PS2). 53

3.13 Raman spectra of porous silicon samples (a) 20 min sample, heated upto 495°C. (b) 20 min sample, heated upto 760°C. 55

3.14 IR absorption spectra (a) 20 min sample, unheated (b) 30 min sample, unheated (c) 20 min sample, heated upto 495°C. 58

3.15 Deconvolution of IR spectrum of Fig. 3.14 curve (a) for SiH, SiH_2, and SiH_3 peaks 59

Chapter 1

Introduction

Porous silicon (PS) is a spongy phase of Si, normally generated by anodization of single-crystal Si in HF solutions at moderate current densities. The porous silicon is characterized by a structure consisting of a great number of micro-pores (diameter < 2 nm), meso-pores (2-50 nm) and macro-pores (> 50 nm).

Porous-Si was discovered in 1956 by Uhlir [1] during electrochemical etching of silicon in HF solution with silicon as the anode. A brittle, spongy, threadlike structure was obtained exhibiting a variety of pore geometries within an otherwise crystalline material. The observed morphologies vary from a uniform network of fine interconnected pores to linear and wide pipelike pores. The pore size and shape depend upon dopant type (n or p), the dopant concentration in the silicon substrate, the anodization current density, and HF concentration. The properties of PS layers were studied extensively because of their potential use in electronic isolation technologies such as silicon-on-insulator (SOI) and fully isolated porous oxided silicon (FIPOS).

Porous-Si was, in a sense, rediscovered by Canham in 1990 [2] when efficient visible red photoluminescence (PL) at room temperature was obtained from this material.

In view of the fact that the development of Si-based opto-electronics has been severely limited by the indirect nature of silicon energy bandgap, this discovery has triggered worldwide research efforts to understand this behaviour and explore new applications. Various models have been proposed to understand the origin of photo-

luminescence as discussed in later sections. While the origin of PL is still debated, the existence of this interesting effect is well established. Junctions have been made and the electroluminescence (EL) has been clearly demonstrated from the porous silicon structures [3, 4]. Thus prospects of using porous silicon as opto-electronic material are well established. Light emitting diodes, laser and new blue-green display devices based on silicon are future possibilities.

However, in order to use porous silicon to make any reliable devices, major problems are encountered due to the thermal degradation behaviour of PL emission. It normally degrades with time in oxygen or moisture containing environment [5, 6]. IR studies have shown that the PL intensity is strongly correlated with silicon dihydride (SiH_2) surface species [7, 8]. In contrast, other studies have suggested that neither SiH nor SiH_2 is essential for the observation of PL in anodized Si [9]. In particular, degradation of EL intensity with time has been an outstanding problem [3, 4]. PS is a high resistivity material and under EL current injection conditions, the local temperature of the junction can be very high due to heating. This leads to the degradation of the device. Thus the thermal stability of the samples is crucial to the reliable and long lasting performance of PS devices.

In this work, we have attempted to understand the thermal degradation behaviour of porous silicon using a variety of characterization techniques. In particular, *in situ* mass spectroscopic thermal effusion techniques has been employed to analyze the nature of species evolving from the porous silicon as a function of heating temperature. Heating rate effect and porous silicon layer thickness effects on thermal effusion were studied in detail. Raman and infrared spectroscopies were also performed on porous silicon sample for microstructural understanding of the material of sample.

In the following sections, we briefly describe the formation of porous silicon by various techniques. A summary of optical behaviour and characterization of porous silicon layers is presented. Finally, the motivation and objectives of the present work are stated.

1.1 Etching of Si-Surface

Porous silicon layer is obtained by etching the silicon surface by various methods. A brief summary of etching techniques are given below.

1.1.1 Electrochemical Etching

Electrochemical etching was historically is the first method and most commonly used for the preparation of porous-Si [1]. The mixtures of HF and C_2H_5OH of different concentrations (e.g. 1:1 by volume) is kept in a teflon electrochemical cell. The electrical contacts are made through Pt electrode which is biased negative. Low resistivity Si wafers acts as an anode with positive voltage applied to it. A current of few tens of mA/cm^2 is passed.

The thickness and porosity of porous silicon layer depend on total etching time, current density and the strength of the etchants. This method is also known as anodization. In the present work, porous silicon layers have been prepared using this technique and more experimental detail will be presented in Chapter 2.

1.1.2 Photochemical Etching

In photochemical etching laser light [10] or very strong light from tungsten lamp (500 W) [11] is irradiated on a sample which is kept inside a teflon cell containing etching(HF) solution. This irradiation activates the reaction and porous Si is obtained. Typically 10-15 min is enough for the completion of the reaction.

1.1.3 Chemical Etching

HF-HNO_3 based solution is kept in a teflon cell without electrical biasing the Si-wafer [12]. Porous-Si is obtained by chemical etching and this porous-Si have similar properties as porous-Si obtained from electrochemical etching. Chemical etching with $NaNO_2$ in HF [12] and CrO_3 in HF [13] have also been reported in literature.

1.1.4 Spark Erosion Technique

A high voltage is applied between a clean Si wafer and silicon electrode for a spark to take place. The electric sparking erodes Si-surface and porous-Si is obtained [14]. This porous-Si has also exhibited similar properties as porous-Si obtained from usual electrochemical etching.

1.2 Porous Silicon Formation Mechanisms

A satisfactory theory for porous silicon formation should be able to explain the preferential pore formation in comparison to uniform etching, as well as the observed transition in surface morphologies with varying experimental parameters. To explain pore formation, majority of growth models do not concern themselves with the exact dissolution chemistry, but invoke physical arguments to explain the influence of anodizing conditions on porous silicon morphologies. This is because of the fact that the detailed dissolution chemistry of silicon is complex and not understood clearly. Therefore, the basic formation mechanism are still in dispute. Several dissolution mechanisms have been proposed, an excellent review of which is found in article by Smith and Collin [15].

The major models proposed to explain porous silicon formation can broadly be categorized into two classes. The early models are mainly phenomenological, invok-

ing arguments based on the electric field redistribution in silicon electrolyte system. Recently several computer simulations have been performed, which try to model the silicon-HF system with simplified parameters which bear some correlation to the experimental conditions [16].

The proposed mechanisms involve the formation of semiconductor depletion layers [15], or the two dimensional quantum size effects [17, 18]. However, common to all models is the role of hole carrier density in the Si material. Therefore, doped p-type Si is the favourite material for anodization to form porous silicon. Porosity in the material depends upon the anodic dissolution process, which is limited by the charge supply from the Si electrode and not by the ionic diffusion in the electrolyte. There exists a critical current below which porous silicon is formed. At higher current densities than this, electropolishing is observed. PS formation current densities are in the range of 10-100 mA/cm^2. For an n-type silicon, intense illumination is required for high minority carrier (hole) generation rate. In this case, the current density is a function of applied bias and the resulting micropores tend to be identical to those on a p-type substrate.

1.3 Luminescence Behaviour

The visible photoluminescence of porous silicon at room temperature and related optical properties have invited maximum scientific attention because of its potential technological applications in optoelectronic devices. There are three types of optical properties of porous silicon as given below.

1.3.1 Photoluminescence

Porous silicon emits light in the range 650-850 nm when irradiated with UV-light [2]. It is easily observed (even with naked eyes) at room temperatures. Many types of excitation sources such as Ar^+ and He-Cd lasers, and filtered UV lamps light have been used to observe PL. By using suitable optics, monochromator and detectors, the PL spectra are obtained. PL peak varies from bright red (~700 nm) [2] to blue-green (~500 nm) [19, 20] depending upon the anodization parameters and post fabrication treatments. Linewidths are typically found to be of the order of 100-150 nm.

This striking phenomenon has initially been attributed by Canham to the formation of surface passivated Si quantum wire arrays [2]. An observed blue shift in PL peak was ascribed to the increase in porosity and consequential decrease in the model was proposed by Brandt *et. al.* [21] that observed PL phenomena can be attributed to a Si-backbone polymer, namely siloxene ($Si_6O_3H_6$). This suggestion was supported by a comparison of PL, IR and Raman spectra of porous silicon and that of siloxenes. Other groups claim that surface dihydride passivation [5, 7, 8], molecules attached to the Si surface [22] or amorphous Si [23, 24] are responsible for the room temperature photoluminescence of porous silicon.

The photoluminescence of porous silicon is very sensitive property and it is affected by ambient air [25], water vapor surrounding [26], oxidation in N_2, or H_2, etc. atmosphere [27]. Interesting effects on the photoluminescence of porous-Si are observed, if the pores are filled with some other material like Yb [28] or Er. C_{60} deposition in pores of porous-Si has been reported recently [29], and it is observed that many other peaks of photoluminescence also originate due to C_{60} plantation in porous-Si.

Temperature affects photoluminescence very strongly and there is almost no photoluminescence above 500^oC [30]. There is no clear explanation for this experimental observation. But it is argued that the vanishing of photoluminescence is due to desorp-

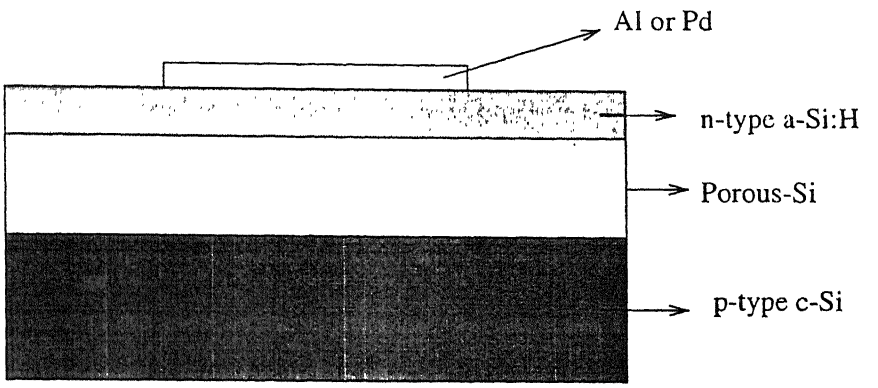


Figure 1.1: pn-hetereojunction fabricated by using porous silicon layer

tion of silicon hydrides from porous-Si [31]. Thermal desorption studies on porous-Si may help in understanding of chemical structure of this material. The prediction can be made from desorption data about chemical species like SiH_n, SiF_n, H_2, etc. recorded with temperature which are responsible for photoluminescence.

1.3.2 Electroluminescence

Porous-Si exhibits electroluminescence (EL). Structures which have been studied include Schottky diodes employing Au [32], Al [4], pn-homojunction [33], and pn-hetereojunctions [34]. These devices show rectifying characteristics. However, all exhibit varying degrees of parasitic series resistance. In Schottky diode structures, the non-ideality is believed to be due in part to non-optimum electric contact at the interface between the porous-Si layer and the metal or semiconductor.

A typical pn-heterojunction electroluminescent device structure is shown in Fig. 1.1 [35]. This pn-junction shows ordinary pn-junction I-V and rectifying characteristics. The electroluminescence is to found decrease as applied current is decreased. The

peaks of electroluminescence and photoluminescence nearly coincide at ~700 nm (visible range). This points to Porous-Si applications in optoelectronic devices at industrial level in near future. However, the degradation phenomena and lifetimes of these EL devices need to be investigated before they gain acceptability.

1.3.3 Electrochemiluminescence

The electroluminescence of porous-Si in wet condition (i.e. during anodization in aqueous solutions such as KOH) is called electrochemiluminescence (ECL). ECL is less efficient than EL. This may be because of a more efficient carrier injection mechanism as the contact area is larger. However, ECL is not permanent and is quenched rapidly because of oxide formation on the surface which cuts off electrical contact between crystallites. A similar, but relatively permanent ECL has been observed on cathodically polarized n-type porous-Si in contact with $S_2O_8^{-2}$ solutions [36]. In this case, the oxidation of the material is avoided.

1.4 Vibrational Spectroscopy

Vibrational spectroscopy is used for finding the bonding configuration between atoms in a material of a sample. In our experiments, we have used Raman shift to determine silicon bonding and infrared spectroscopy to see the presence of silicon hydrides and oxide bonds. A brief introduction to Raman spectroscopy and infrared spectroscopy is given here.

1.4.1 Raman Spectroscopy

Raman effect is an inelastic collision between the incident photon and the molecule, when quanta of vibrational energies are emitted or absorbed as a result of collision. When light (with frequency ω_o) interacts witha medium, an oscillating dipole moment is induced, which in turn, emitts the spectrum of scattered radiation consisting of many pairs of side bands symmetrically disposed around the elastically scattered radiation. The origin of inelastic scattered components is attributed to the modulation of polarizability of the medium by the molecular or crystal vibration. This inelastic scattering of light is used as a sensitive vibrational spectroscopic tool to investigate structure, symmetry, and dynamical properties of solids, liquids, and gaseous system.

The scattered radiation found is to have frequency lower or higher than the frequency of incident radiation. The phenomenon in former case is known as Stokes Raman scattering while in the latter case as anti-Stokes Raman scattering. Two types of these events are illustrated in Fig. 1.2.

In Fig. 1.2(a), the system of particle (say molecules) is unexcited initially. An incident radiation photon at frequency ω_e is observed and a Stokes photon at $\omega_{SR} = \omega_e - \omega_v$ is emitted simulaneously. To conserve energy, the molecules excited to state ω_v as shown in Fig. 1.2(b), an anti-Stokes photon at $\omega_{ASR} = \omega_e + \omega_v$ may be emitted along with two de-excitation of the molecule from v = 1 to v = 0. Since anti-Stokes emission depends on the number of molecules being in initially in excited state, it is weaker than Stokes emission.

The modern theories of Raman effect explain the phenomenon in terms of creation and anhilation of photons. For example, in first process (Fig. 1.2 (a)), a photon of frequency $\omega_{SR} = \omega_e - \omega_v$ is created, while one photon of frequency ω_e is anhilated resulting in the excitation of the of the molecule from v =0 to v = 1. Similarly in the other process (Fig. 1.2 (b)) a photon of $\omega_{ASR} = \omega_e + \omega_v$ is created along with the annihilation of a photon of frequency ω_e resulting in the de-excitation of the molecule from v = 1 to v =0.

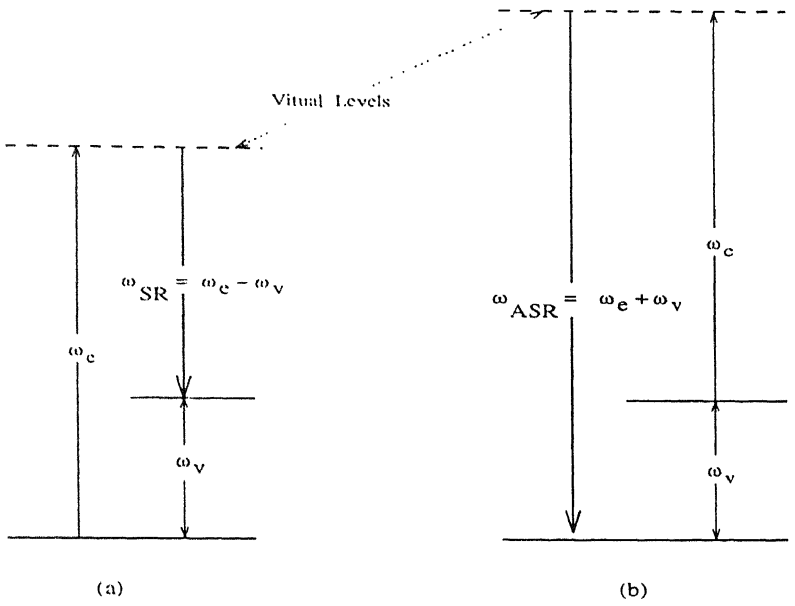


Figure 1.2: Stokes Raman and anti-Stokes Raman effects

Raman scattering is usually weak in intensity, hence a high intensity source is needed for its observation. For this reason, a stimulated interest in its studies and application arose only in past decades after the invention of laser sources.

Raman effect is the result of interaction between electromagnetic waves and incident dipole moment. Hence it is fundamentally different from IR absorption. The two phenomena are complementary to each other in providing information about the dynamics of a system.

1.4.2 Infrared Spectroscopy

The IR absorption is a phenomenon involving interaction between electromagnetic radiation and matter. To a first approximation, it occurs through changes in electric dipole moment of the molecular unit arising due to its excitation to a higher energy level. It may also occur through changes in electric moments of higher order, magnetic

moments, etc. However, the absorption through such interactions is generally found to be negligibly weak. Frequencies of vibrations in molecules and solids match with the energy of IR photons, hence enough information about the vibrations in these systems may be collected from IR absorption spectra.

Experimentally, when the broad band infrared (IR) radiation incidents on the medium, a part of the incident radiation, matching with the characteristics vibrational frequencies of the medium, gets absorbed and rest is transmitted. The analysis of the transmitted (or reflected) light in the IR (600-4000 cm^{-1}) region provides information regarding the vibrational levels, symmetries, and structural characteristics of solids, liquids, and gaseous system.

1.5 Statement of the Problem

Since the proposal of Canham[2] that visible photoluminescence in porous silicon is due to quantum size effect, there has been a very large number of studies on various properties of this material. A whole array of characterization techniques have been used to obtain complimentary information, specially those related to photoluminescence. However, studies on thermal stability of the material and nature of chemical species present in the material has not been studied in any detail. Since the mode of preparation of porous silicon involves electrochemical bath containing acids and alcohol, many different chemical species are only to be expected in the material. Further, the material being porous has large surface area and hence it is all the more likely that chemical species present on the internal surface of the material would influence its properties. Various studies on optical and transport properties of the material suggest that process at the surface play a dominant role.

With this in view, it is important to have a reliable and quantitative method of studing surface desorbed species in porous silicon and their relation to thermal stability of the material. In this work, we have prepared porous silicon and heated

them in vacuum to analyze various species effusion out using mass spectroscopy. It is possible to obtain insights regarding mechanism of desorption and origin of various species by studying thermally stimulated effusion spectroscopy (TSES) of each individual species. A computer controlled Quadrupole Gas Analyzer has been used to set up TSES. We go on to show that monitoring evolution of hydrogen from the sample can play central role in understanding of desorption mechanism. We also use complimentary techniques of infra-red absorption spectroscopy and Raman spectroscopy to obtain microstructural information.

Chapter 2

Experimental

2.1 Sample Preparation

This chapter gives detail of porous silicon sample preparation and experimental procedure followed to characterize them. The samples were prepared in our laboratory. This is very long process and requires many steps to be followed. First of them is to clean Si-wafer, so that no impurity is left on its surface. To make electrical contact for electrochemical etching, Al or some other appropriate metal has to be deposited on back surface of Si-wafer. The etching and drying is the last step for sample preparation. We have described the detail in the following sections.

2.1.1 Si-Wafer Cleaning

The Si-wafer is cut into appropriate sizes (e.g. 2 X 2 cm^2 or 1.5 X 1.5 cm^2 for our experiments). The Si-wafer is dipped in acetone and ultrasonically cleaned for 5-10

min. The wafer is taken out and kept in air for 1-2 min for vaporization of acetone and then dipped in trichloro ethylene and again ultrasonic vibration are given for 5-10 min. The wafer is then dipped in dilute-HF and ultrasonic vibration for 2-5 min are given. After that the wafer is rinsed in deionized water for few minutes and dried in desiccator. This way, the wafer is cleaned and made ready for Al-deposition.

2.1.2 Al-Deposition on Si-wafer

Back surface of the Si wafers is coated with Al using vacuum evaporation techniques. Fig. 2.1 shows the schematic diagram of Al-deposition set-up. There is large beljar which is vacuum proof on its base by rubber ring. Vacuum is created by rotary vacuum pump of the order of 10^{-2} to 10^{-3} Torr. Al foil is heated in a W-filament coil. When the appropriate vacuum is reached, W-filament is turned on. Si-wafer(s) which are cleaned as described above, are kept facing back surface toward the W-filament. The evaporated Al gets deposited on lower surface of Si-wafer. If vacuum is not high enough, oxides of Al and Si are formed in the vacuum chamber. This oxide formation is highly undesirable because not only Si-wafer surface gets oxidized, but also oxide of Al is deposited on Si-wafer surface and as we know silicon oxide is an insulator, a poor electric contact will be formed. Therefore, high vacuum is very essential in Al-deposition.

2.1.3 Thermal Annealing of Al-deposited Si-wafer

Al-deposited silicon wafer does not produce good porous silicon sample, if Al-deposited silicon wafer is not annealed appropriately. This is because of electric contact is not made uniformly on its back surface. To make good ohmic contact, Al deposited silicon wafer is annealed before anodization as described .

Fig. 2.2 shows the schematic of annealing set-up. It has a hollow cylindrical

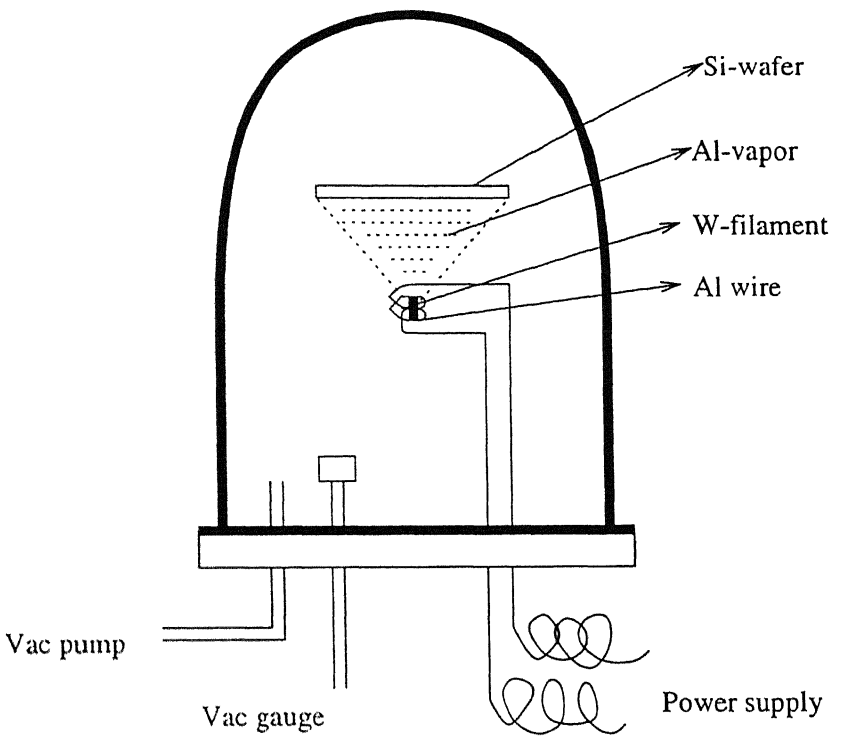


Figure 2.1: Schematic diagram of Al-deposition set-up

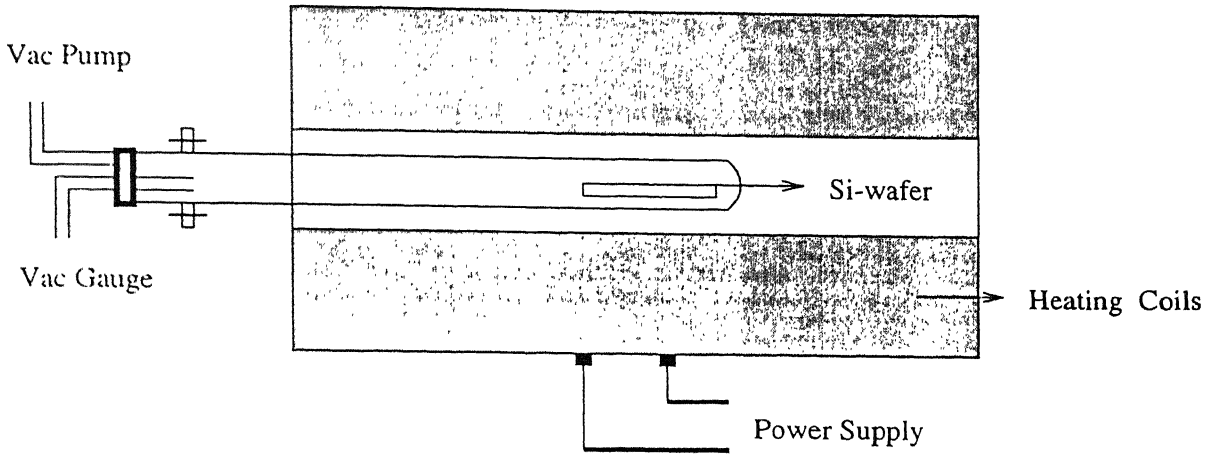


Figure 2.2: Schematic diagram of annealing set-up

furnace. Temperature distribution inside it is uniform. Al-deposited silicon wafer is placed in a large quartz tube which is connected to vacuum pump and vacuum gauge.

Vacuum of the order of 10^{-5} to 10^{-6} Torr is created first inside the quartz tube before inserting it into the furnace. If the quartz tube is inserted into the furnace without appropriate vacuum, the wafer would get oxidized The temperature of the furnace is set at 250-350°C. Annealing time is 1-2 hours for all Al-deposited silicon wafer. When the annealing time is over, the furnace is turned off and quartz tube is left to cool down inside the furnace. Finally, when the temperature is around room temperature the vacuum pump is also turned off and the sample is taken out. Care is taken not to turn off vacuum pump, unless the temperature of furnace is around room temperature because the leaks at joints oxidizes the sample inside at elevated temperature. This annealed wafer is ready for electrochemical HF etching.

2.1.4 Electrochemical Etching of Si-Wafer

Al-deposited and thermally annealed in vacuum Si-wafer is used for electrochemical etching. Fig. 2.3 shows the schematic detailed diagram of teflon cell used for electrochemical etching. The Si-wafer is kept on metal anode stand. An o-ring of appropriate size is kept on Si-wafer; in our case, we have used 1 cm diameter o-ring. The anode with the wafer is tightened with a big teflon screw to make junction leak proof. If this screw is not tightened properly, HF solution leaks to back surface of the wafer.

The mixtures of HF and C_2H_5OH (1:1 by volume) is poured in to the teflon cell. This whole set-up is kept on a teflon stand to facilitate electric connections. The electric contacts are made with Pt electrode which is negative and dipped in HF solution. Si wafer is used as the positive electrode (or anode). Typical current supply used is 10 mA dc. The wafer diameter is $\sim$1.5 cm (therefore the current density is $\sim$ 5.6 mA/cm^2). The etching time is varied between 10-30 mins for different Si-wafers in all of our experiments.

When electric power supply is turned on, we observe gas bubble coming out from etching solution. This is the indication that the etching process is going on the surface of the sample. We also observe changing color of Si-wafer as the process proceeds. The sample looks grey after around 5 minutes.

2.1.5 Drying Process of Fresh Porous Silicon Sample

The electric contacts are disconnected when the etching time is over and HF solution is poured out. Since porous silicon layer is a very delicate structure, to avoid damage to the sample care is taken in pouring out HF solution and in drying process. DI-water is poured in carefully and the cell is left for 10-20 min. Now DI-water is also poured out and the sample is taken out by removing bottom screw.

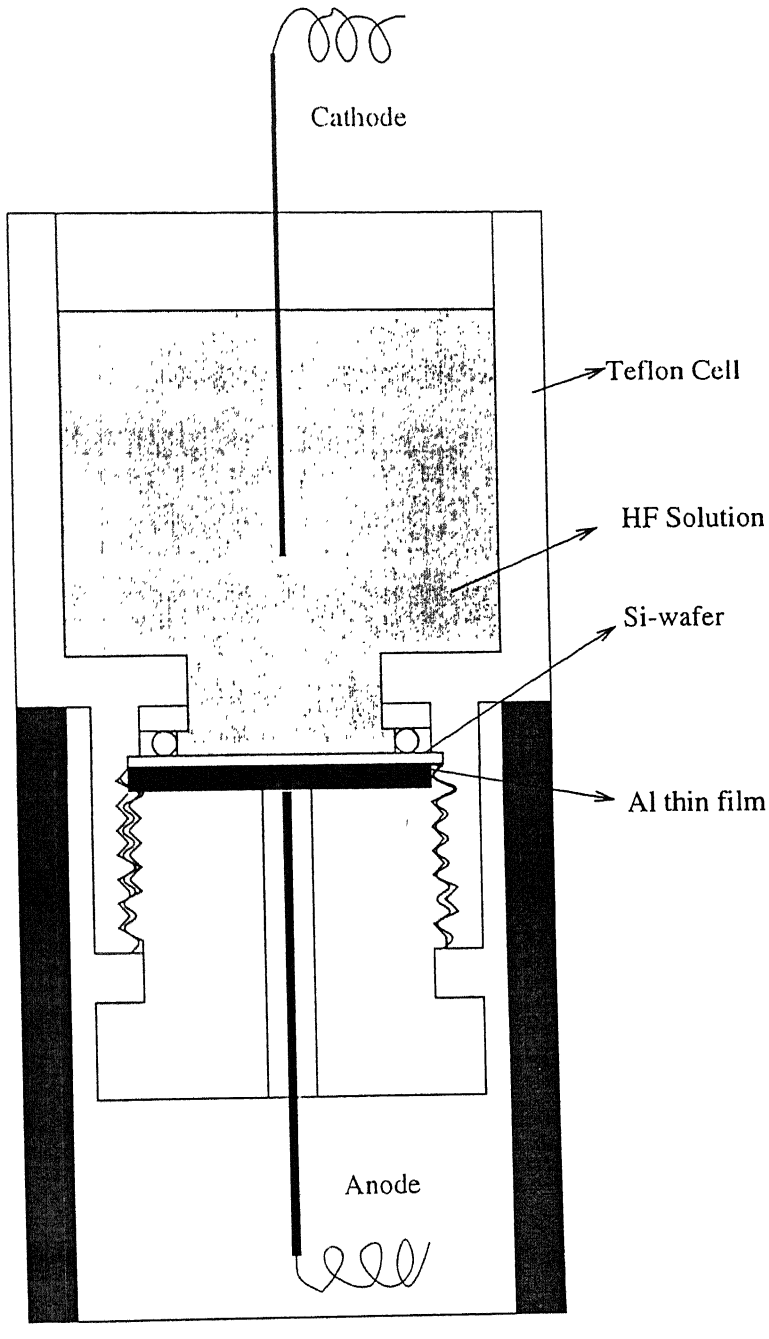


Figure 2.3: Schematic diagram of teflon cell

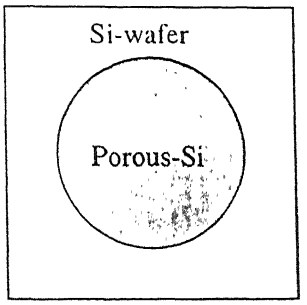


Figure 2.4: Porous-Si Sample

The typical prepared porous silicon sample is shown in Fig. 2.4. The central circular portion which looks dark grey is porous silicon layer. The thickness of this layer is of the order of few microns. Finally, samples are dried and stored in desiccator. This sample is ready for any experimentation after 30-60 min.

2.2 Mass Spectroscopic Thermal Effusion Set-up

Mass Spectroscopic Thermal Effusion Set-up is used to measure chemical species which effuses out from heating of sample in high vacuum. The set-up used in experiments lab was assembled in our lab. It consists of the following main parts. A quartz tube inside a cylindrical furnace, Quadrupole Gas Analyzer(QGA), PC Interfac and a thermocouple. We have described the detail of these parts below.

2.2.1 Quartz Tube with a Furnace

A quartz tube of outer diameter 14.4mm and length 7 inch is connected to QGA and a turbo molecular pump. High vacuum of the order of 10^{-6} Torr is created by the turbo molecular pump. Temperature is measured by thermocouple which is

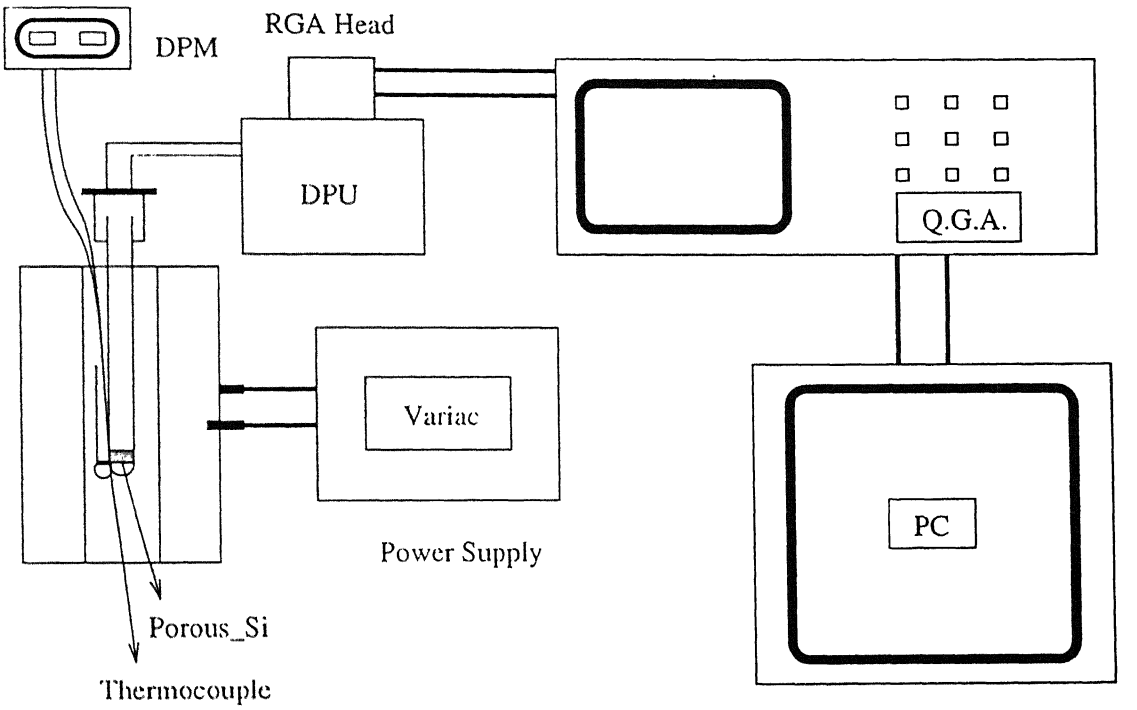


Figure 2.5: Schematic diagram of Mass Spectroscopic Thermal Effusion Set-up DPM : Differential Penning Meter(for temperature measurement), RGA : Residual Gas Analyzer, DPM : Differential Pressure Units, QGA : Quadruple Gas Analyzer, PC : Personnel Computer

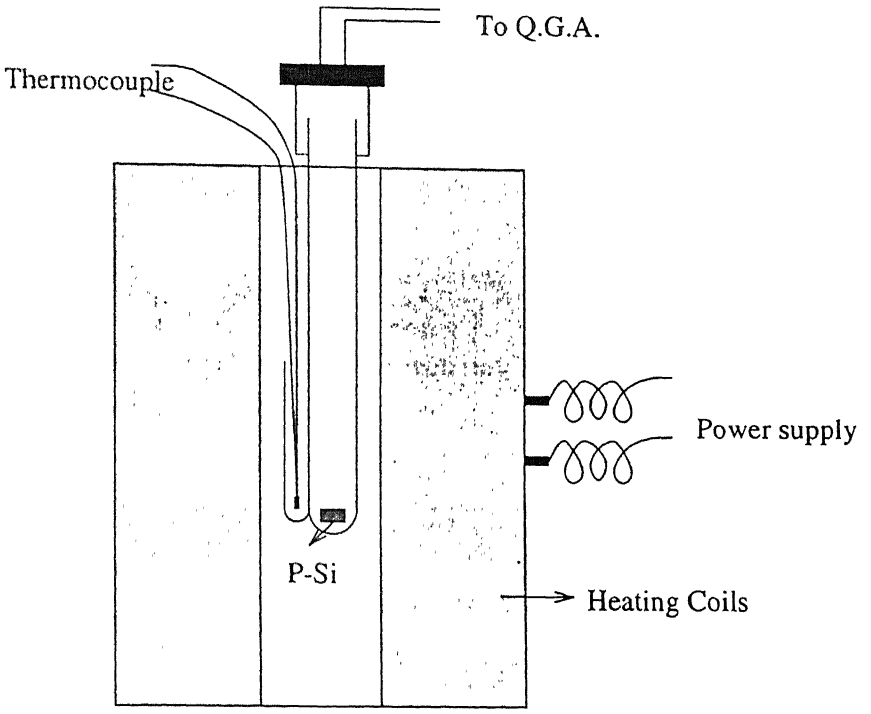


Figure 2.6: Schematic diagram of heating tube with furnace

kept in another quartz tube of inner diameter of 3mm. This tube is attached to the bigger tube which contains the porous silicon sample Fig. 2.6 shows very clearly this configuration. This whole assemble is kept in furnace symmetrically. The power is supplied by variac. The voltage of it, hence its temperature is controlled manually. The detail of how linear temperature is obtained, is described in section 2.2.3

2.2.2 Quadrupole Gas Analyzer

Quadrupole Gas Analyzer is used to analyze gases by converting to their ions and then detecting m/e ratio. Since m/e of different gases may be same, so we can not determined them uniquely. A determination normally involves physical arguments as well. We describe briefly the mechanism of QGA below.

The head of quadrupole gas analyzer have four metal rods in pairs of two. The oscillating electromagnetic field is generated by applying rf-voltage. The molecules (radicals) of coming gases are converted to ion(s) in ion chamber and collected in the collector chamber. The parameters of gas molecules for characterization are their masses and their charges. This instrument only determines m/e of different constituents as the path ions traverse depends on both, mass and charge.

It can work in two modes. In first mode, the entire spectrum of partial pressure of gases vs. m/e of 1-200 amu can be recorded and in second mode, partial pressures of maximum 12 gases with different m/e as function of time is recoreded. We have used both the modes in our experiments. A PC(286) is interfaced to QGA. The interfacing program (written in BASIC) reads the partial pressure at specified temperature from QGA and stores in a given file and directory.

2.2.3 Calibration of Temperature

The sample is heated in vacuum ($\sim 10^{-6}$ Torr) inside a quartz tube. The temperature of furnace is controlled manually using variac. As the voltage is increased, the temperature increases non-linearly. To obtain linear heating rate, the voltage is set high and then slowly increased. For example, to get linear heating rate of 18°C/min., initial voltage is set at 44 volts and then one volt is increased per minute, The typical heating rates obtained in these experiments are shown in Fig. 2.7. It is clear that the heating rate can be controlled to a good accuracy.

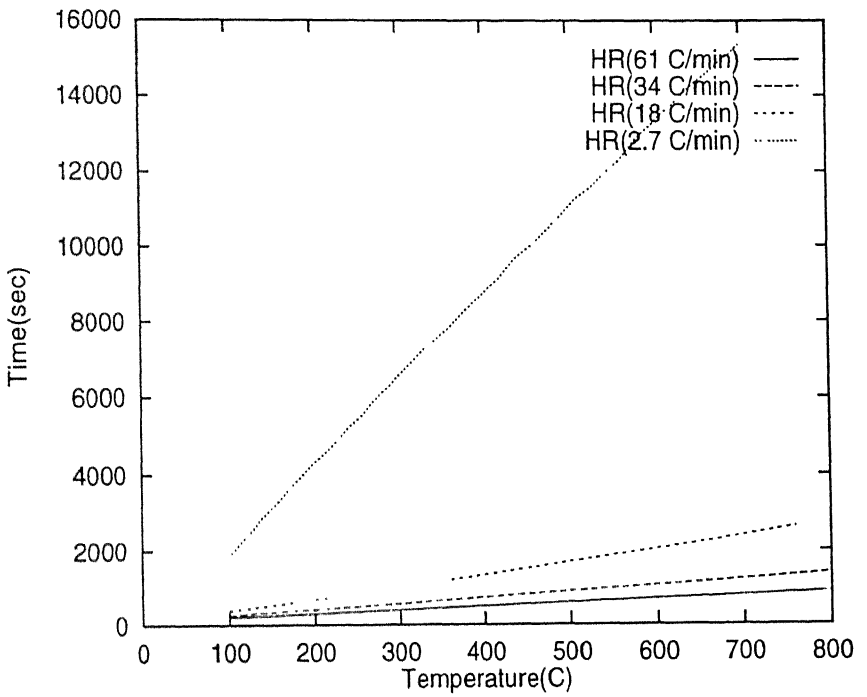


Figure 2.7: Typical heating rates used in thermal effusion PS samples

2.3 Characterization of Porous Silicon Sample

To characterize porous silicon samples prepared in our laboratory, we used following techniques.

2.3.1 Mass Spectroscopic Thermal Effusion

In this work Mass Spectroscopic Thermal Effusion (MSTE) technique has been used extensively. MSTE set-up has already been described in section 2.2. The experimentation is as follows.

A porous silicon sample was first put in to the quartz tube. (cf. Fig. 2.6). All connections of set-up was made vacuum leak proof by using appropriate o-rings. Vacuum pump is turned on and when the vacuum is approximately $\sim 10^{-6}$ Torr, we turn on the furnace also. The sample is heated with linear heating rate by changing the voltage of variac at regular time interval manually. For detail see section 2.2.3. The temperature was measured with a thermocouple and data was recorded.

The partial pressure of number of chemical species were recored by a PC interfaced to QGA. The data was recorded at regular interval of temperature. We have taken temperature interval in our all experiments to be 10°C. The temperature range was 100-800°C. Plots were taken for all 12 ions. The detail of ions are given in Table 3.1.

2.3.2 Raman Spectroscopy and Photoluminescence Measurements

Crystallinity of porous silicon was analyzed by Raman Spectroscopy. The theory of Raman Spectroscopy is described in chapter 1, section 1.4.1. These Experiments

performed on SPEX-1877 Triplemate (Raman Spectrometer). Laser light (wavelength 514 nm) is shined on the porous silicon sample and Raman shift is stored by a PC automatically in appropriate range of wavelength. Raman spectra in our experiments were taken for many samples, heated partially or completely, and unheated.

2.3.3 Infrared Spectroscopy

Infrared Spectroscopy experiments was performed on PERKIN ELMER 1320. The wave number was changed from 600 to 4000 cm^{-1}. We recorded IR transmission spectra for 20 and 30 min samples of porous silicon. The back surface of sample which was coated with Al was removed before the IR spectra was taken as Al absorbs IR light.

2.4 Peakfit Analysis

The peakfit analysis is a software package which is used to fit the various types of curves like Gaussian, Lorentzian, Voigt, etc. on experimental data. Peakfit is very easy to use, as it is a menu driven package. First the graph is plotted and on that curve fitting is done by adjusting the width and the height of the curve and its type itself for example like Gaussian or Lorentzian or some other type The base line subtracts the initial and residual effects present.

The number of peaks and peak type are selected depending on the nature of data peaks. When the adjustment of peaks and base line is over, software repeats iterations for the best fit. These fitted curves gives detailed information about data peaks like precise peak position, FWHM, percentage area under various peaks etc.

We have used peakfit software in our all peak analysis and the peak position, FWHM, and percentage area under peaks were found. A typical analysis for hydrogen

thermal effusion peaks using peakfit is shown in Fig. 2.8. It is interesting to note that the two effusion peaks can be fitted to Gaussians. In this manner, we obtain the peak position, FWHM, and area under the peaks quite accurately.

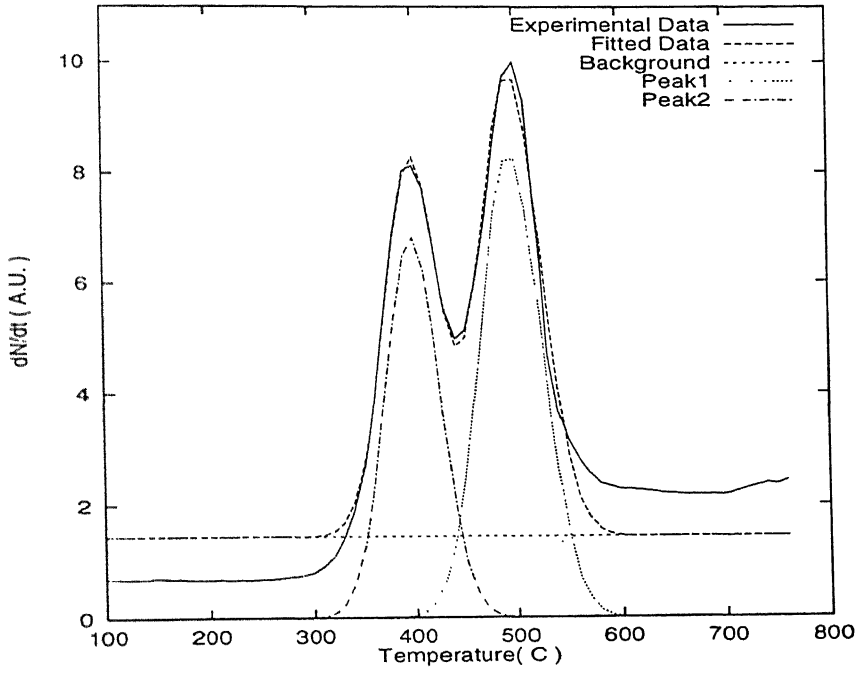


Figure 2.8: A typical peakfit analysis for hydrogen peaks.

Chapter 3

Results and Discussion

In this chapter, we present the results of characterization of porous silicon involving photoluminescence, thermal effusion studies, infrared and Raman spectroscopies. The main emphasis is on mass spectroscopic analysis of effusion of species from the samples with heating in vacuum.

3.1 Photoluminescence from Porous Silicon

As described earlier, the observation of room temperature photoluminescence (PL) from porous silicon is the reason for hectic research in past few years in porous silicon area.

In fact, PL is the first characterization step required to ascertain the quality of sample. All sample prepared by us were found to be bright red/orange under UV light from a mercury lamp seen with the naked eyes. Room temperature photoluminescence spectroscopy was used for detailed characterization of the samples under various heat treatments.

Fig. 3.1 shows the photoluminescence spectra recorded on a sample PS2 in as-prepared and heat treated states. PS2 was prepared for etching time of 20 min with a constant current density ~5.6mA/cm^2. The diameter of the sample was ~15 mm. The sample was cut in to four pieces. The first piece of this sample was not heated at all. The second piece was heated upto 495°C in vacuum (~10^{-6} Torr) at a heating rate of 6.2°C/min. The third part of the sample was heated upto 760°C in vacuum at a heating rate of 18°C/min.

After heating the sample in vacuum at the desired temperature, heating furnace was switched off and the samples were allowed to cool down to room temperature under high vacuum. This kind of heating treatment is to distinguished from the more common isothermal annealing. PL spectra shown in Fig. 3.1 were recorded under excitation illumination from an Ar^+ laser operating at 514 nm with the micro-Raman setup described in Chapter 2. Care was taken to keep the laser intensity low in order to avoid the heating of the sample. All three spectra were recorded in a single stretch under same operating conditions, such as laser intensity, slit widths, etc.

We observe from Fig. 3.1 that a broad photoluminescence peak centered at ~701 nm (1.77 eV) is obtained on the as prepared porous silicon sample . Full width at half maximum (FWHM) for this peak is ~135 nm (350 meV). On heat treated sample (~ 500°C), PL intensity is found reduce without significant shift in the peak position (~700 nm, FWHM ~150 nm). In contrast, no PL was observed on the 760°C heat treated sample.

The photoluminescence of our sample is typical of those observed by others. It is customary to report at least one PL spectra in any report on porous silicon. Therefore, plethora of experimental data does not allow a direct comparison to be quoted. In general, the position of PL peak is found to be at ~1.7 eV with broad spectrum width of ~0.3 eV. The peak positions depend upon the microstructure of the sample and the sample history. Our photoluminescence data is simular to those reported by Hadj Zoubir *et. al.* [37] and Tsai *et. al.* [7] on porous silicon samples in their thermal treatment studies. A comparison of the experimental data with the

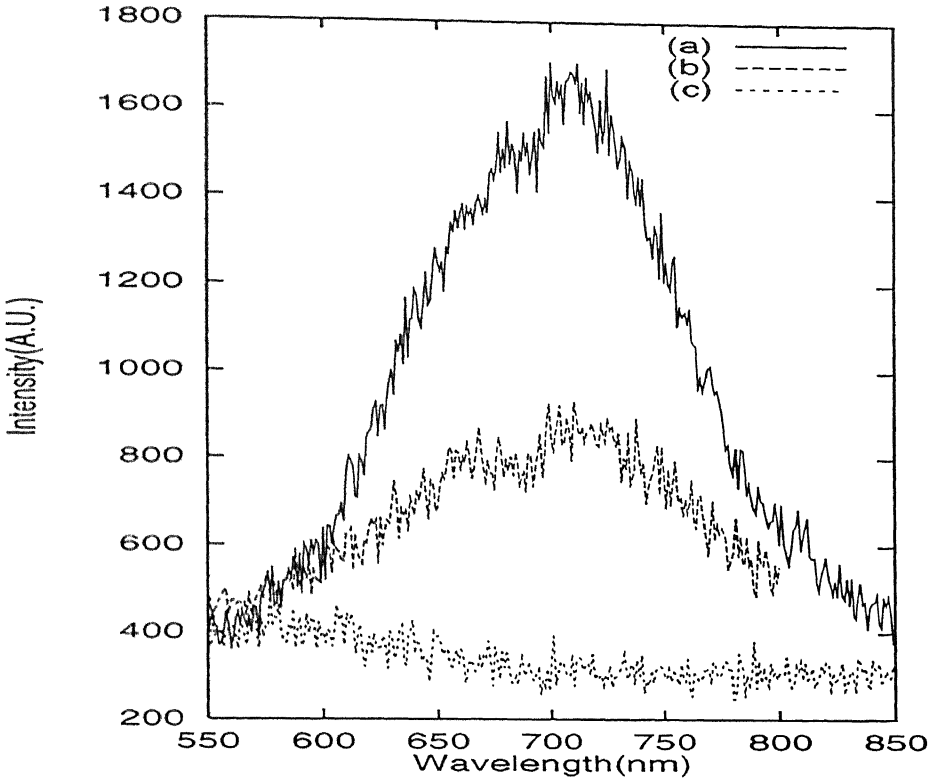


Figure 3.1: Photoluminescence spectra from 20 min porous silicon sample. (a) unheated. (b) heated upto 495°C/min with heating rate 6.2°C/min. (c) heated upto 760°C with heating rate 18°C/min.

theoretical simulations of John and Singh [16] suggest a mixture of quantum wires and dots with a Gaussian size distribution.

Degradation of photoluminescence on thermal annealing in vacuum is well reported [37, 38] Photoluminescence degradation is shown to start as soon as 200°C annealing temperature is reached [37]. Photoluminescence is seen to become completely quenched by annealing upto ~450°C [37, 7]. In contrast, photoluminescence intensity is seen to increase with a red-shift in peak position when samples are annealed in air [39]. In our case substantial luminescence is observed in samples heated upto ~500°C. However, photoluminescence is totally quenched in sample heated upto ~760°C.

3.2 Mass Spectroscopic Thermal Effusion

The technique constitutes of heating the sample in vacuum and observing the effusing out species. Coupled with the mass spectrometric analysis of these species, thermal effusion offers powerful capabilities to investigate thermal induced effects. We have employed this technique for detailed analysis of heat treatment behaviour of porous silicon.

Fig. 3.2 shows a mass spectrum in the range of 1 to 100 amu at constant temperature of 460° on a typical porous silicon sample. We observe various clusters of peaks around mass to charge rario (m/e) of 2, 15, 30, 42, 55, 70, and 82 with some other small peaks.

The assignment of various m/e numbers to the chemical species is not unique and requires physical interpretation. We make these assignments based on the probability of the presence of species and their cracking patterns. For example, the peak at m/e = 2 is assigned to the molecular hydrogen, even though He^{2+} also has same m/e. He^{2+} is not expected to be present in any significant amount in our porous silicon sample, as the preparation of porous silicon is based on electrochemically etching of crystalline Si wafer in HF solution. Similarly, the peaks around m/e = 15 and 31 are attributed to CH_3^+ and SiH_3^+ respectively. Higher m/e peaks are due to fluorides of silicon.

From this large number of peaks, a set of twelve mass numbers were selected for measurement during time/temperature dependent effusion scans. Table 3.1 shows a list of these mass numbers along with their assignments.

The table contains only singly ionized ions with m/e in increasing order, as in ionic chamber mostly singly charged ions are produced. We set these m/e number in QGA and data was stored for these ions only during thermal effusion of porous silicon. The sample temperature and gas partial pressures were continuously recorded during heating. Thermal effusion spectra were measured at different heating rates (

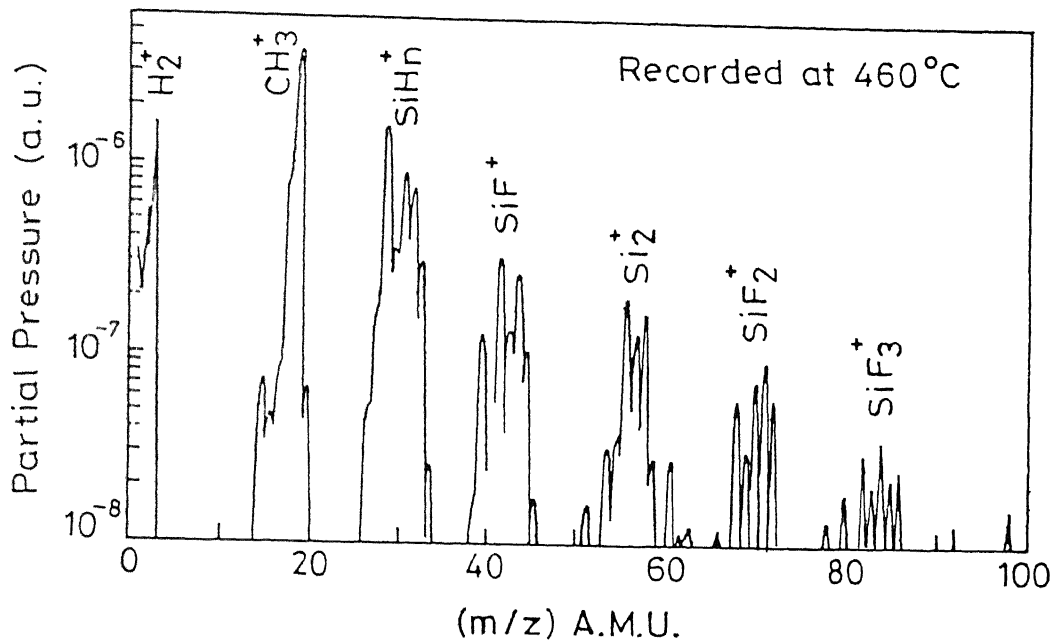


Figure 3.2: Mass spectra of thermal desorption from porous silicon. The peaks are centralized around m/e 2, 15, 30, 42, 55, 70, and 82 with some other small peaks

Table 3.1: The ions traced in our mass spectroscopic thermal effusion experiments

Serial no.	Ions	(m/e) of Ions
1.	H^+	1
2.	H_2^+	2
3.	CH_3^+	15
4.	H_2O^+	18
5.	HF^+	20
6.	SiH^+	29
7.	SiH_2^+	30
8.	SiH_3^+	31
9.	SiH_4^+	32
10.	SiF_2^+	66
11.	SiF_3^+	84
12.	AlF_3^+	85

Fig. 2.7) on pieces of same samples. In addition, samples of different thicknesses produced at different etching times were also studied at fixed heating rates. The partial pressures of effusing species at the pumping port represent a measure of the effusion rate (dN/dt) as the pumping speed of turbo-molecular pump over a wide range of pressure is constant.

3.2.1 General Behaviour

We plotted data for all 12 types of ions separately as a function of temperature. Fig. 3.3 shows thermal effusion spectra from sample PS2 heated at a rate of $\beta = 16^{o}$C/min. We show the evolution of H_2, SiH, SiH_2, SiH_3, SiF_2, and SiF_3. These were the only species showing a thermal stimulated effusion pattern. Clear peaks are observed in the temperature range of 150-600°C. Thermal effusion of molecular hydrogen (H_2) is seen to dominate the spectra. The low temperature (LT) peak for hydrogen is centered around 396°C and the high temperature (HT) peak around

496°C. The FWHM for these peaks were found to 57 and 71°C, respectively. The area ratio under the peaks for LT to HT

Contribution from hydrides of silicon (SiH, SiH_2,and SiH_3) peak at the same temperature of 360°C indicating a common desorption mechanism responsible for the observation of these peaks. Another smaller peak at 175°C is observed in effusion spectrum of SiH. Thermal effusion from the fluorides of silicon (SiF_2 and SiF_3) peaks at a higher temperature of 600°C. Here, we focus only on the general features observed in the thermal effusion spectra. We shall come back to the detailed description and mechanism in later sections.

As seen in Fig. 3.2, many other species also desorb from the porous silicon surface. However, thermal effusion rates for these species, such as HF, AlF_3, CH_3, and SiH_4 when plotted as function of temperature do not show any particular thermal activated behaviour. We have shown plots for CH_3 and SiH_4 in Fig. 3.4 and in Fig. 3.5 respectively. These figures show that effusion rates of CH_3 and SiH_4 decreases continuously as the temperature of the sample increases. This behaviour indicates that these species are not chemically bonded to the porous silicon network. Therefore, these ions comes out very fast initially and latter slowly showing no peak at all. If they were bonded to the surface of the sample, they would have shown some thermally stimulated peak behaviour, as the desorption from surface requires definite amount of energy. It may be pointed out that oxygen is observed at same mass number as SiH_4 and hence the desorption curve in Fig. 3.5 may have initial contribution from oxygen also.

General features observed in the mass spectroscopic effusion spectra are consistent with the only paper reported on porous silicon [37]. The presence of chemically bonded hydrides and fluorides in the effusion spectra suggest that most of the silicon atoms on HF-treated silicon surface are covered with hydrogen and small amount of fluorine. The surface silicon atoms are bonded to one, two or three hydrogen or fluorine atoms and it must be expected that, during thermal desorption, these hydrogen or fluorine atoms desorb from the surface directly or after recombination,

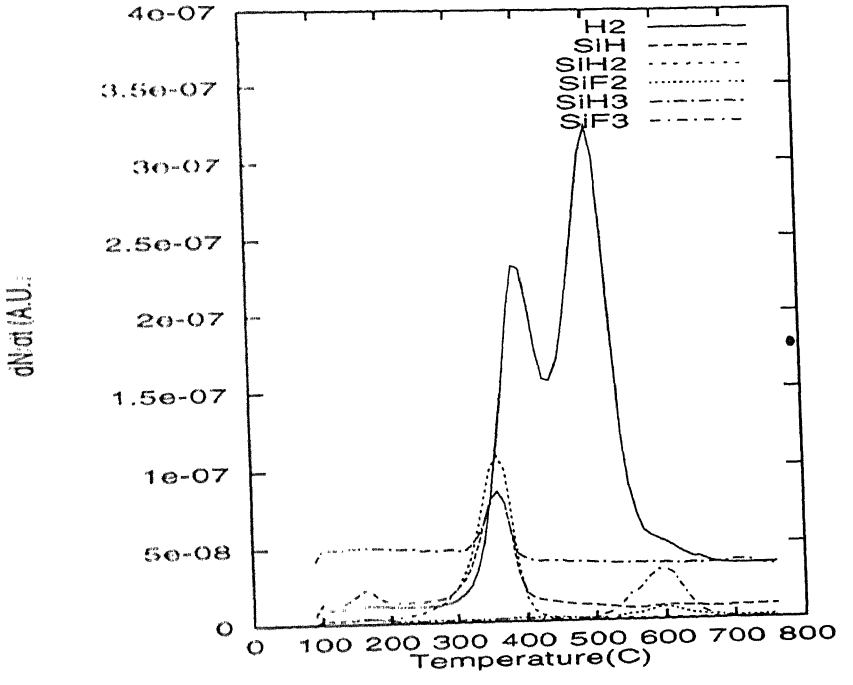


Figure 3.3: Effusion curve for thermal desorption from 20 min sample (PS2) heated at the rate of 16°C/min. The clear peaks for hydrides of silicon appear at 360°C. Hydrogen peaks are at 396°C and 496°C.

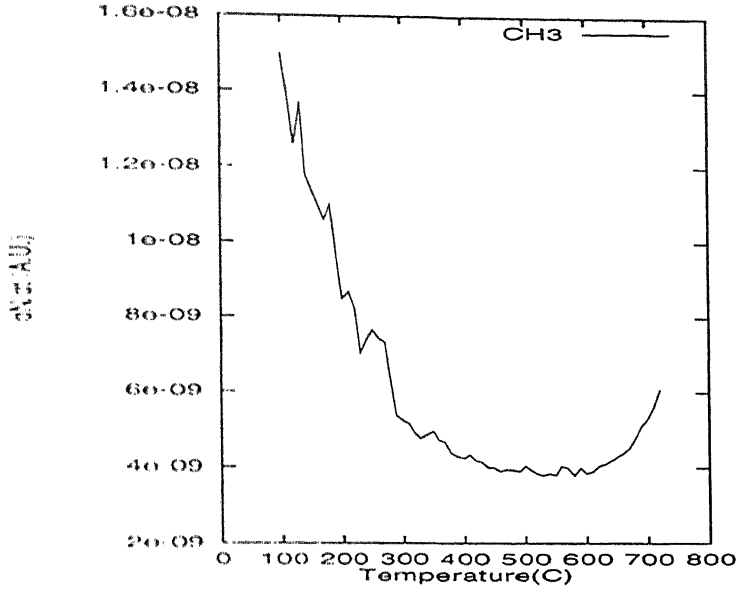


Figure 3.4: Effusion curve for thermal desorption of CH_3. It is found to decrease continuously as the temperature increases.

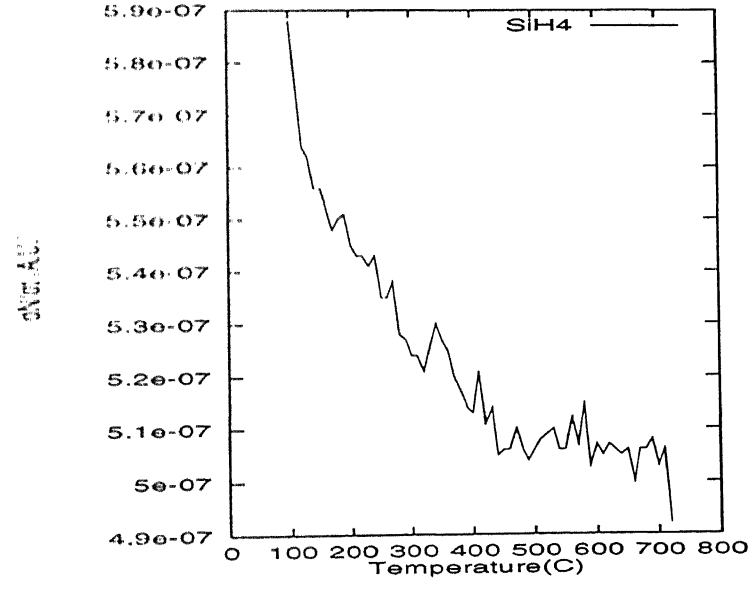


Figure 3.5: Effusion curve for thermal desorption of SiH_4. It is also found to decrease continuously as the temperature increases.

with silicon atoms. The molecules desorbing in the largest quantity are the hydrogen molecules (Fig. 3.3.)

The fact that SiH_3 desorbs before the effusion of hydrogen is in agreement that SiH_3 molecules are slightly more mobile than hydrogen atoms [40]. But in this case, all hydrogen present at the surface would escape in the SiH_n species and, next, there should not be any release of molecular hydrogen. Moreover, the desorption energies the three species (viz SiH, SiH_2, and SiH_3) must be different. The release of SiH_3 units needs to break only one Si-Si bond, the energy for which is slightly lower than that of Si-H bond. On the other hand, the release of SiH_2 or SiH units directly from the surface needs to break two or three Si-Si bonds which is not energetically favorable. As the evolution of SiH and SiH_2 are perfectly identical to that of SiH_3, it is more likely that these species are originated in the cracking of SiH_3 in the quadrupole mass analyzer.

3.2.2 Thermally Stimulated Desorption Kinetics

Before we go on to discuss our experimental results, we present the relevant method of analysis of thermally stimulated desorption process.

The kinetics of gas desorption processes follow a rate equation ([41])

$$\frac{dN}{dt} = A(1-N)^n \exp\left(-\frac{E_a}{RT}\right) \tag{3.1}$$

where N is the fraction of gas atoms evolved by overcoming the free energy barrier E_a. A is pre-exponential factor, n is order of reaction and R is gas constant. If temperature rises at a constant heating rate, the evolution rate will first rise to maximum value and then return to zero when all the available gas for effusion has been exhausted. The temperature of maximum evolution rate (T_m) informs about the stability or bonding strength of the evolving atom/molecule to the network. By

differentiating equation (3.1), we get

$$\frac{d}{dt}\left(\frac{dN}{dt}\right) = \frac{dN}{dt}\left[\frac{E_a\beta}{RT^2} - An(1-N)^{n-1}\exp\left(-\frac{E_a}{RT}\right)\right] \tag{3.2}$$

Maximum evolution rate occurs at a temperature T_m defined by equation (3.2) equal to zero.

$$\frac{E_a\beta}{RT_m^2} = An(1-N)_m^{n-1}\exp\left(-\frac{E_a}{RT_m}\right) \tag{3.3}$$

The amount of hydrogen left in the sample $(1-N)_m$ is not readily determined from the evolution pattern. However, equation (3.2) can be integrated to obtain a resulting exponential integral. This way, a satisfactory approximation is obtained.

$$\frac{E_a\beta}{RT_m^2} = A\exp\left(-\frac{E_a}{RT_m}\right) \tag{3.4}$$

For order of reaction and initial concentration of unity, equation (3.4) modifies to

$$\nu_o\exp\left(-\frac{E_a}{kT_m}\right) = \frac{E_a\beta}{kT_m^2} \tag{3.5}$$

Hence, for first order desorption kinetics, the activation energy for desorption (E_a) may be determined from T_m by the equation (3.5), where $\nu_o \sim 10^{13}s^{-1}$. Now differentiating equation (3.5) and neglecting small quantities, we get

$$\frac{d\left(\ln(\frac{\beta}{T_m^2})\right)}{d\left(\frac{1}{T_m}\right)} = -\frac{E_a}{R} \tag{3.6}$$

regardless of order of reaction.

At low heating rates, more time is available for the evolution process. Therefore, net amount of gas (to be same for two heating rates) will evolve at lower temperature only. In evolution spectrum, the peak (T_m) occurs at lower temperature with a decrease in heating rate (β). By measuring the variation of T_m with β, a graph can be plotted between $\ln(\beta/T_m^2)$ vs $1/T_m$. The slope of this curve will give the activation energy E_a using equation (3.6).

Diffusion of gas atoms in compact material may limit the evolution rate. This can be detected by measuring evolution spectra on identical samples of different thicknesses. With the increase in PS layer thickness, the increase in diffusion length results in a shift of the evolution peak to higher temperature. For a diffusion limited evolution, the hydrogen concentration profile c(x,t) across the film must be compatible with the diffusion equation

$$\frac{\partial c}{\partial t} = D(t)\frac{\partial^2 c}{\partial^2 t} \tag{3.7}$$

with a time dependent diffusion coefficient $D[T(t)]$. Solving the diffusion equation for out-diffusion from a PS layer of thickness d at a constant heating rate and expressing D is terms of a diffusion pre-factor D_o and a diffusion energy E_d by

$$D = D_o \exp\left(-\frac{E_d}{kT}\right) \tag{3.8}$$

we get

$$\ln\left(\frac{D}{E_d}\right) = \ln\left(\frac{d^2\beta}{\pi^2 kT_m^2}\right) = \ln\left(\frac{D_o}{E_d}\right) - \frac{E_d}{kT_m} \tag{3.9}$$

For two different thicknesses d_1 and d_2 of the identical samples and corresponding peak temperatures T_{m1} and T_{m2}, equation (3.9) gives

$$\ln\left(\frac{d_1^2 T_{m2}^2}{d_2^2 T_{m1}^2}\right) = \frac{E_d}{k}\left(\frac{1}{T_{m2}} - \frac{1}{T_{m1}}\right) \tag{3.10}$$

Thus, from measurements of T_m as a function of the layer thickness d for the samples prepared under identical conditions and heated at a fixed heating rate β, the activation energy for diffusion can be determined.

3.3 Desorption of Hydrogen

As seen in Fig. 3.3, the molecules desorbing from porous silicon in the largest quantity are the hydrogen molecules. The hydrogen release occures between 300°C to 600°C with two prominent peaks. A detailed analysis of hydrogen desorption kinetics from silicon surfaces was carried out by Gupta *et. al.* [42] in the pre-photoluminescent porous silicon period. Combining the results of it in situ FTIR and thermal effusion measurements, the low temperature and high temperature peaks were identified as hydrogen desorbing from dihydrides (SiH_2) and monohydride (SiH), respectively [42].

To investigate the nature of hydrogen incorporation on porous silicon and its thermal release mechanism, we changed the heating rate (β) from ~3C°C/min to ~60°C/min on same sample. In addition, thermal stimulated effusion spectra (TSES) from samples having different thicknesses (obtained by changing the anodization time) were studied at a fixed heating rate.

3.3.1 Effect of Heating Rate on Hydrogen Desorption

Fig. 3.6 shows the effusion spectra corresponding to molecular hydrogen from sample PS1 (10 min anodization time). Four spectra shown were recorded from the four pieces of the same sample at different heating rates of β = 2.7, 18, 42, and

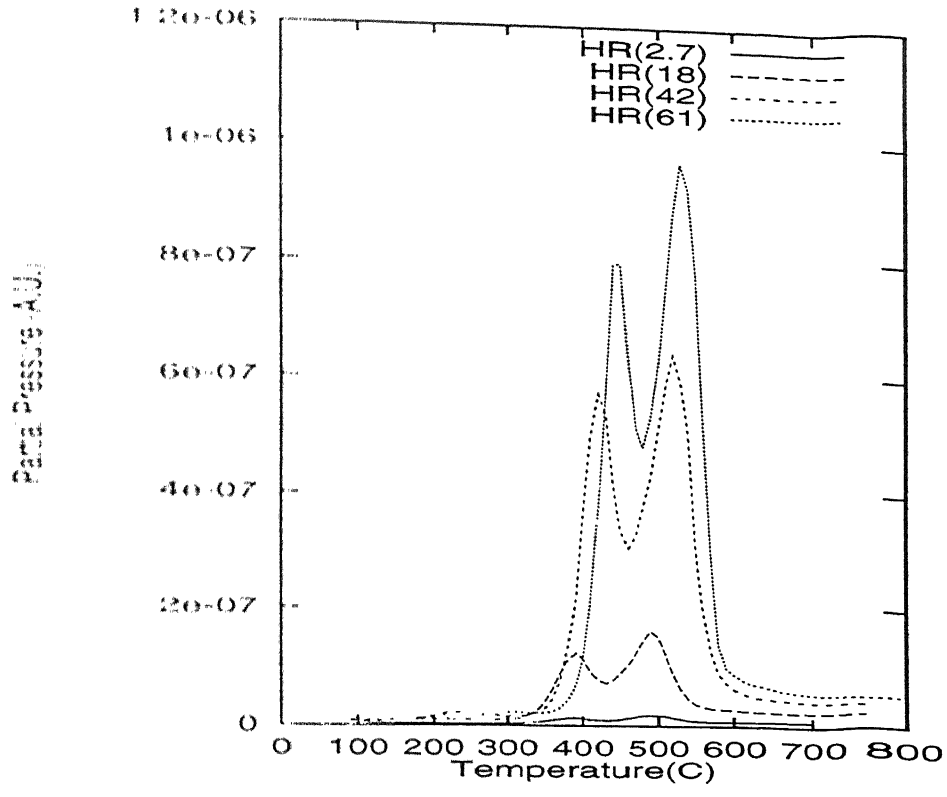


Figure 3.6: Hydrogen effusion curves for thermal desorption from porous silicon

61°C/min. With increase in heating rate, consistent shift to higher peak energies (T_m) is observed for both LT and HT peaks. Peakfit analysis shows both peaks to be symmetrical around T_m at all heating rates. Further, the ratios of areas LT and HT peaks remain constant at 2:3.

On increasing the heating rate, time available for effusion of the gas is smaller. Therefore, maximum (T_m) in effusion rate ($\frac{dN}{dt}$) is encountered at a higher temperature. Therefore, the results observed are physically expected for thermally stimulated processes. In Fig. 3.6, we observe molecular hydrogen in the mass spectra and record of atomic hydrogen at m/e = 1 does not show similar behaviour. Therefore, a mech-

anism is required for formation of molecular hydrogen before it is detected by mass spectrometer. The formation of hydrogen molecule in the gas phase after detrapping from the sample is energetically unfavorable and hence it formation can be ruled out. Here it may be pointed out that the multilayer studies using hydrogen and deuterium in amorphous silicon films have shown molecule formation in the film itself [43].

Various steps involved in the evolution of hydrogen are: detrapping of hydrogen from its bonded site, recombination of hydrogen atoms to form H_2 and out diffusion of molecular hydrogen. Porous silicon contains large surface area to volume ratio ($200m^2/cm^3$). Due to such large porosity the effusion process is not expected to be limited by diffusion.

As described earlier, LT peak corresponds to hydrogen from dihydride of Si (SiH_2) and HT peak to the monohydride (SiH). Desorption from monohydride species is anticipated to be governed by second order rate kinetics [42]. Two hydrogen atoms from two adjacent silicon monohydride species must recombine to produce H_2. Further, by using *in situ* FTIR spectroscopy during isothermal annealing, Gupta *et. al.* observed a second-order desorption kinetics from the silicon dihydride species also [42].

A detailed thermal analysis of non-isothermal kinetics curves obtained at constant heating rates gives for the order of the reaction gives an approximate relation [44]

$$n = 1.26(\frac{b}{a})^{1/2} \tag{3.11}$$

where a and b are absolute values of the inverse slope at first and second inflection points of the $\frac{dN}{dt}$ curve. Equation 3.11 predicts that the number of gas atoms remained in the sample at peak temperature will decrease as exponent n is decreased. This implies that the evolution peak will become increasingly symmetric as n is decreased [45]. Thus our highly symmetric peaks for LT as well as HT hydrogen evolution from SiH_2 and SiH respectively, also indicate that nature of the desorption process involves a second order reaction kinetics. Further, the shape our thermal effusion

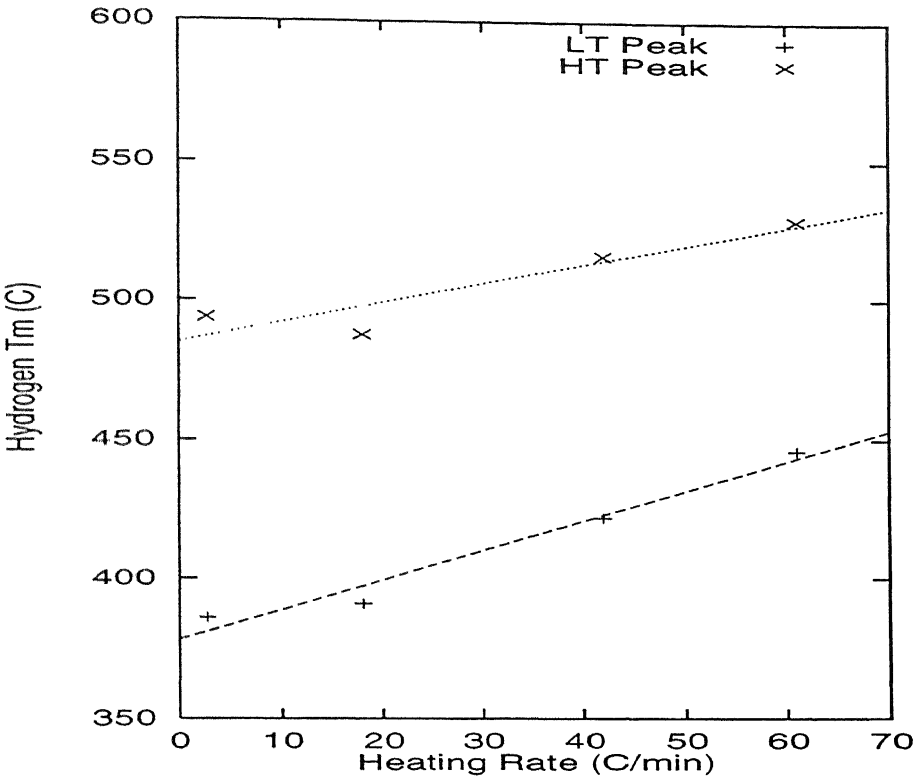


Figure 3.7: Hydrogen peaks shift as heating rate is changed for 10 min sample (PS1)

curves are similar to the theoretically predicted curves using second order reaction kinetics equation ([42]).

Following equation (3.6), which is independent of the order of reaction, we plot $\ln(\frac{\beta}{T_m^2})$ vs $\frac{1000}{T_m}$ for the data shown in Fig. 3.6. Fig. 3.8 shows the Arrhenius plot. Activation energy, E_a, can be estimated from this Arrhenius plot. E_a for LT and HT come out to be 0.8 eV and 2.5 eV respectively.

The activation energy for high temperature peak ($E_a = 2.5$ eV) corresponding to desorption of hydrogen from monohydride of silicon is in good agreement with the values reported in the literature from porous silicon [42] as well as from H_2 desorption

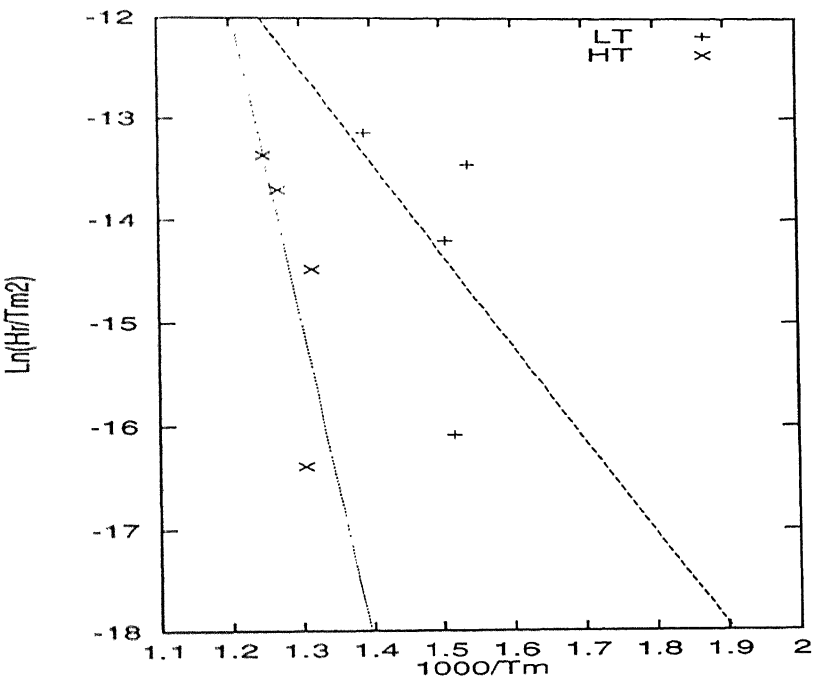


Figure 3.8: Arrhenius plots for 10 min sample (PS1)

from clean Si(111) surfaces [46]. This activation barrier can be understood as the difference between the energy required to break two nearby Si-H bonds and binding energy of a hydrogen molecule using

$$2E(Si-H) = E_a + E(H-H)$$

with the literature values of $E(H-H) = 4.5$ eV and our experimental value of $E_a = 2.5$ eV, Si-H bond energy of 3.5 eV is obtained. This value is within the range of E(Si-H) obtained in amorphous silicon network (3.2 eV, [43]) and E(Si-H) crystalline silicon surfaces (3.58 eV, [42]).

Difficulties are encountered in understanding the low values of activation energy (0.8 eV) required for LT peak corresponding to the release of hydrogen from dihydride (SiH_2).

A similar analysis produces unreasonably low value of Si-H bond energies (2.65 eV) on the SiH_2 surface species. This is lower than expected values of ~3.10 eV [42]. One reason could be uncertainties in the LT peak E_a determination from Arrhenius plot. However, limited β dependent data on other samples also show the same behaviour.

If we assume a first order reaction as assumed in the analysis of LT hydrogen peak from clean Si(111) surface [46], and a widely used approximation [47].

$$\frac{E_a}{kT} = \ln(\frac{\nu_1 T_m}{\beta}) - 3.64 \tag{3.12}$$

activation energy of 1.96 eV is obtained. Here $\nu_1 = \frac{kT}{h}$. This value of E_a is close to the LT peak on a-Si:H (1.9 eV) as well as on surface desorption from c-Si (1.86 eV, [46]).

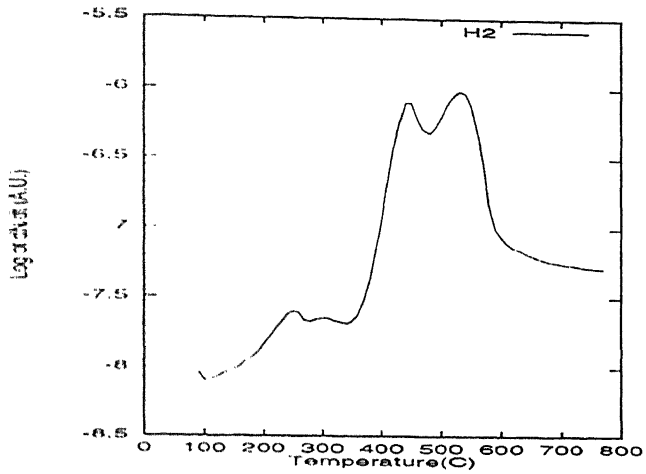
However, as discussed earlier, peak shape analysis of our data in over a dozen effusion spectra from different samples taken at different heating rates shows highly symmetric LT peak. This observation is consistent with the only reported data on porous silicon [37] as well as predicted effusion curve [42]. In contrast, peak shape

of effusion spectrum from clean c-Si is clearly indicative of a first order reaction [46]. In addition, compelling evidence from the *in situ* FTIR analysis also shows a second order reaction kinetics [48]. Therefore, in order to understand the low activation energies obtained by us, the possibility of reconstruction or dimerization of surface silicon atoms can not be ruled out. If desorption is concurrent with reconstruction, the energy gained in the reconstruction process would lower the desorption activation energy barrier. Additional experiments are required to confirm the competing processes.

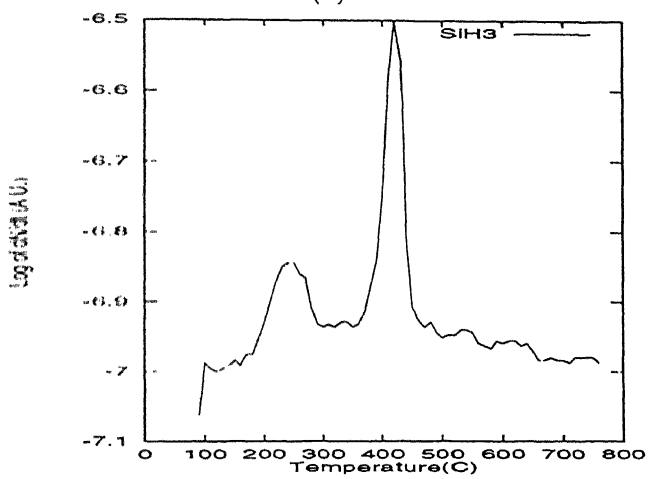
In our case, we have observed PL in the sample, even after heating upto 500°C, i.e., HT peak (Fig. 3.1). There are observations where PL is completely quenched by isothermal annealing at these temperatures [37]. However, there is a general agreement that PL starts degrading at temperatures as low as 200°C [37]. Further, Robinson *et. al.* [49] noted that the two phenomena (disappearance of PL and release of hydrogen) are not simultaneous. The PL intensity may already have reduced before the beginning of hydrogen desorption.

In order to verify this we analyzed our effusion data carefully, and $\ln(\frac{dN}{dt})$ vs temperature was plotted for a typical sample (PS1) at a high heating rate (61°C/min). Fig. 3.9 (a) and (b) show spectra for H_2 and SiH_3 desorption. Clear thermally activated effusion peaks are observed at ~245°C with a slight hump at 300°C. Presence of such low temperature peaks have not yet been reported for porous silicon or surface desorption from crystalline silicon surfaces. Fig. 3.10 shows same observation at different heating rates. Variation of low temperature peak with heating rate yield an activation energy of 0.42 eV.

Interestingly, such low temperature hydrogen evolution peaks have been observed in the thermal evolution spectra of B-doped a-Si:H films deposited at low temperatures [43]. It may be stated that low temperature deposited a-Si:H films are usually density deficient. However, lowering of effusion peaks on doping has been observed even in compact a-Si:H films. This suggests that a similar mechanism from porous silicon cannot be ruled out. Our micro-Raman data on porous silicon clearly shows

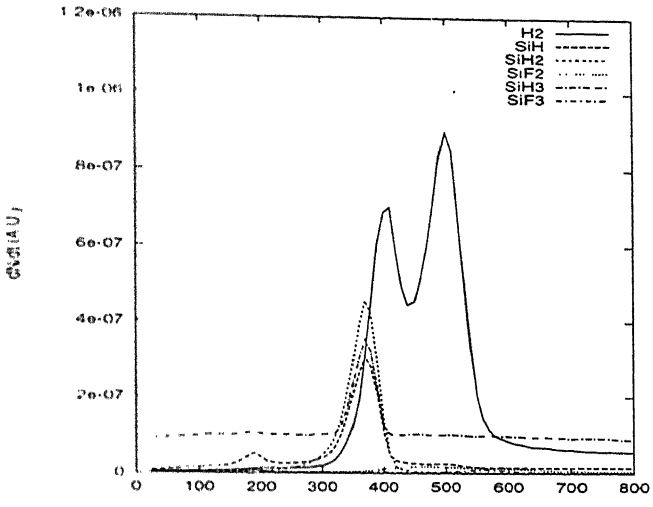


(a)

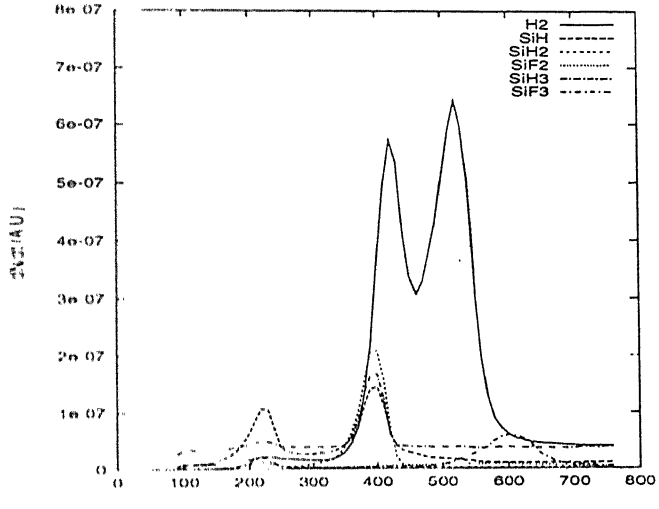


(b)

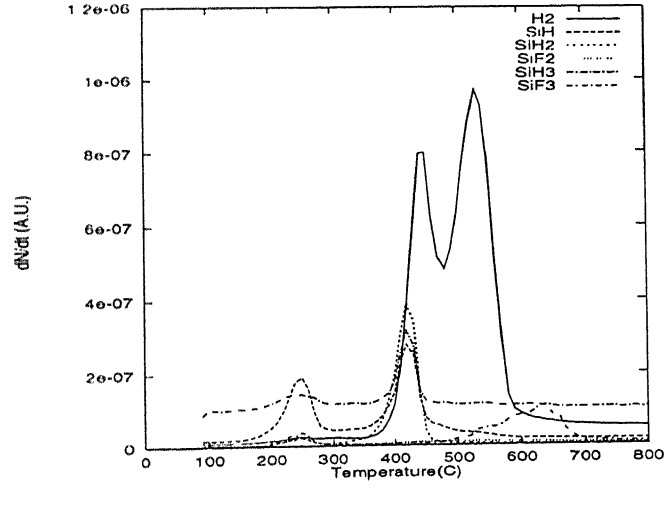
Figure 3.9: (a) H_2 and (b) SiH_3 semi-logarithmic effusion curves for thermal desorption from porous silicon as temperature is increased for 10 min sample (PS1)



(a)



(b)



(c)

Figure 3.10: Effusion curves for thermal desorption from porous silicon for different

the presence of a-Si in the samples (cf. section 3.4). Presence of a-Si:H in highly porous networks is well known and has also been related to the origin of photoluminescence [24, 50]. Boron was also the dopant in our p-type silicon wafer. Therefore, the degradation of PL at lower temperature is indeed related to the detrapping of Si-H species and related structured changes.

3.3.2 PSL Thickness Effect on Hydrogen Desorption

Electric current density and etching time are two important parameters in the preparation of porous silicon sample. If current density is not in a certain range , porous silicon is not formed at all. At lower current densities, there is no anodization while at higher current densities uniform etching (electropolishing) of silicon wafer is obtained.

The thickness of PSL depends on both, current density and etching time. If we keep the current density constant, thickness depends on etching time only. This assumes all other parameters such as temperature, HF solution constituents, and Si wafer type to be same.

We prepared porous silicon samples with etching time of 10, 20, and 30 min. We assume here that the thickness of PSL is linear to etching time i.e. the thickness of 20 min sample is twice as thick as that of 10 min sample. Estimated PS layer thickness are ~6, 12, and 18 μm [51].

Fig. 3.11 shows the thermal effusion spectra for hydrogen from these three samples at approximate heating rates of ~18°C/min and ~34°C/min (Actual heating rates are given in Fig. 3.11). At ~18°C/min heating rate, hydrogen related peaks (LT as well as HT), shift to higher temperature with concurrent increase in their widths. However, the data obtained at higher heating rates show almost no change in peak positions.

We recall the steps involved in the process of thermal effusion of hydrogen:
(i) detrapping of hydrogen atoms, (ii) migration of atomic hydrogen to nearby sites (iii) recombination with another H to form molecular hydrogen and (iv) migration of molecular hydrogen to the surface. We should expect the layer thickness to influence the nature of effusion spectra, if either (ii) or (iv) are rate limiting steps. However, as the surface area is very large with a spongy porous structure, diffusion is not expected to be a rate limiting factor.

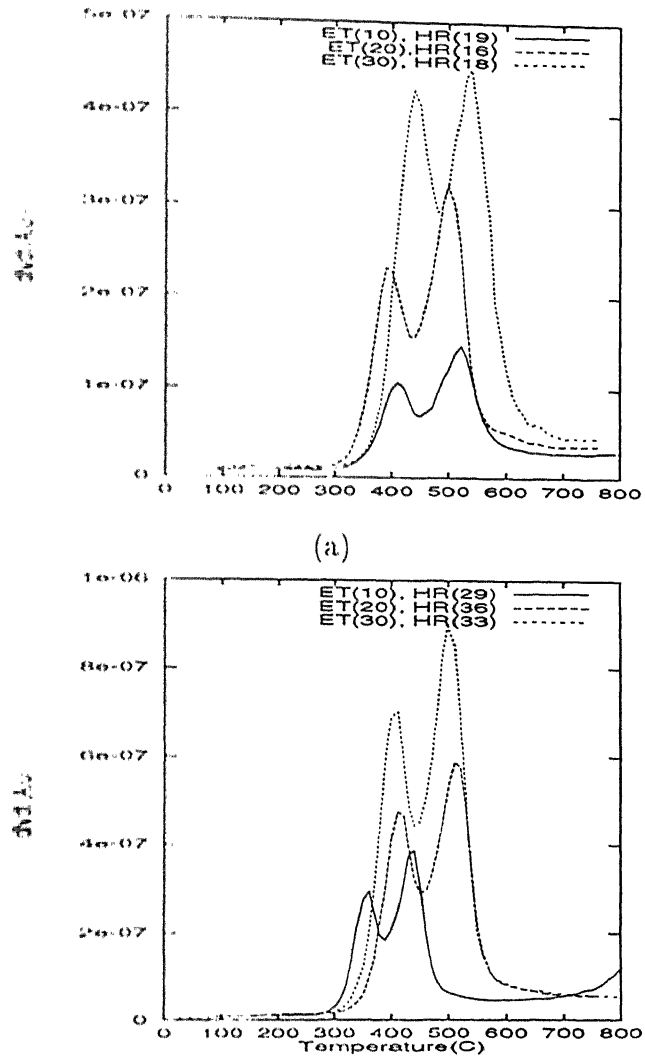


Figure 3.11: Hydrogen effusion curves for thermal desorption from porous silicon as the etching time for sample preparation is changed.

Presence of various surface species and hence thermal effusion spectra are dependent upon the preparation conditions, thermal history, storing environment and aging of the samples. In addition, depth inhomogeneities have been recently reported in porous silicon layers [52]. In addition, careful look at our heating rates (which are manually controlled) also show small difference.

In view of the above discussion, it is not possible to conclude the role of diffusion of atomic or molecular hydrogen in porous silicon from our thermal effusion data. More studies, possibly with capping layers or deuterium markers, are required. However, it may be pointed out that the conclusions derived from β dependence (on pieces of same sample) are highly reliable and show the recombinatory desorption kinetics for hydrogen as discussed in earlier section.

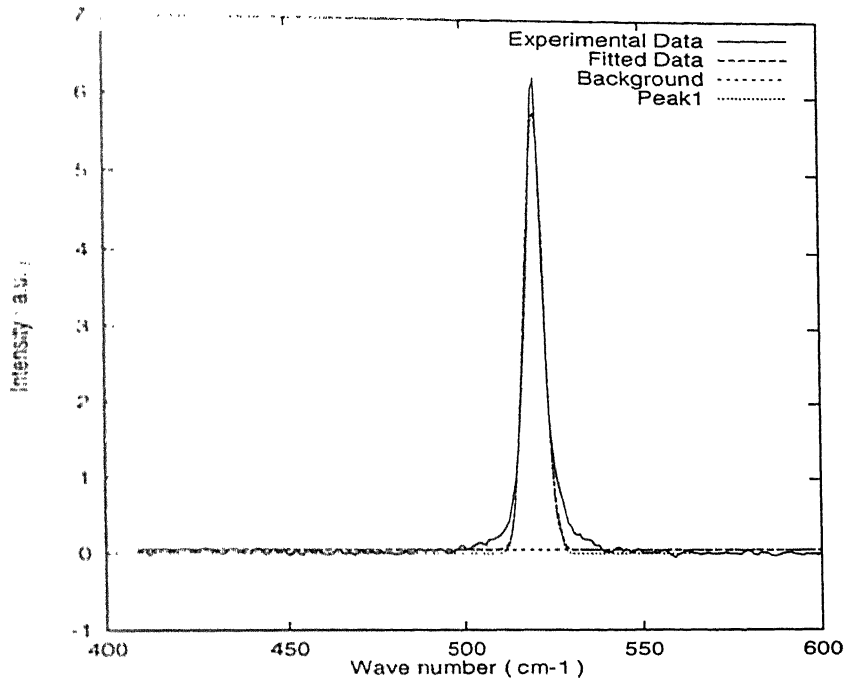
CENTRAL LIBRARY
I. I. T., KANPUR

3.4 Raman Analysis

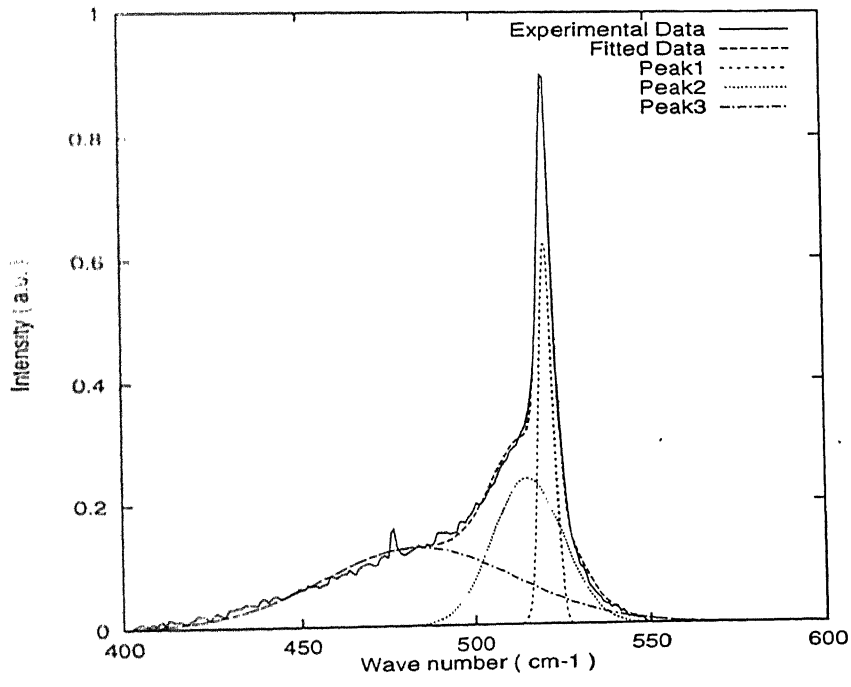
Raman scattering is a powerful non-destructive tool to analyze crystalline size effects in semiconductors. We first state some general features of Raman spectra of silicon. The first-order Raman peak in single crystal Si is observed at 520.5 cm^{-1}. This peak is symmetric in nature and has a width (FWHM) of ~3 cm^{-1}. Variation are observed when the material loses long range order. Iqbal and Veprek [53] reported detailed Raman analysis on the vapor deposited micro-crystalline(μ c-Si) films. As the grain size in μ c-Si decreases below ~200 nm, the Raman shifts decrease to lower frequencies FWHM increases and the peak becomes asymmetric with tail at low frequencies [53]. Raman spectrum of amorphous silicon (a-Si) peaks near 480 cm^{-1} and is usually very broad and weak in intensities [53].

Raman measurements were carried out on the as-prepared and heated porous silicon samples corresponding to the data shown in Fig. 3.12. Fig. 3.12 (b) shows the Raman data on as-prepared sample (PS2, 20 min sample) along with the reference data on crystalline silicon 3.12 (a). Peakfit analysis was carried out. Deconvoluted spectra are shown with dashed lines. In crystalline Si, Raman shift is observed at 520.2 cm^{-1} with a FWHM of 5.5 cm^{-1} (including the instrumental contributions)

As-prepared porous silicon show Raman spectrum typical of porous silicon layers prepared from non-degenerate crystalline silicon [54]. Deconvolution of this spectrum shows three separate peaks. First peak is similar to reference c-Si data and shows contribution from crystallites larger than 200 $\AA$. However, as width of this peak remains same, this peak is more likely due to the contribution from substrate itself. Red-shifted peak at 513 cm^{-1} with a width of 24.5 cm^{-1} is due to the nanocrystallites ($\leq$ 50$\AA$) in porous silicon. Taking the quantum confinement models from the literature [55], crystallite size of ~3 to 4 nm is estimated. A broad peak (FWHM ~60 cm^{-1}), centered at ~484 cm^{-1}, is also observed. This peak shows the contribution due to substantial amount of disordered a-Si phase in the porous silicon. Similar Raman spectrum was observed on as-prepared PS1 sample (not shown here).



(a)



(b)

Figure 3.12: Raman spectra of porous silicon samples (a) Standard c-Si (b) 20 min sample, as-prepared (PS2).

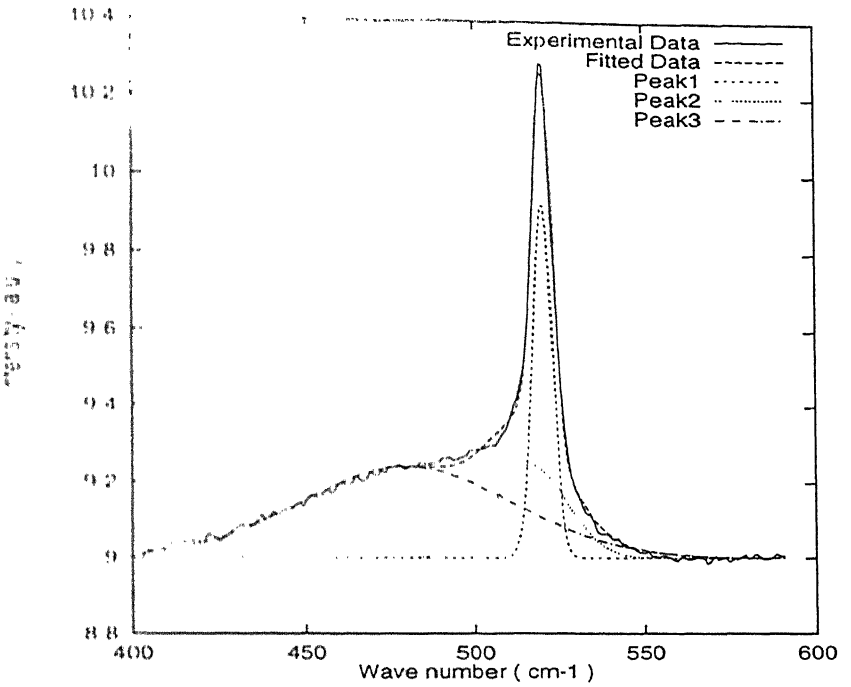
Table 3.2: Peak positions and FWHM obtained from peakfit analysis of Raman spectra of porous silicon samples

PS Samples	Peak 1 (Position, FWHM) cm^{-1}	Peak 2 (Position, FWHM) cm^{-1}	Peak 3 (Position, FWHM) cm^{-1}
As-prepared	520.9, 5	513, 26	484, 60
495 °C Sample	520, 7.4	507, 32.5	473.8, 68
760°C Sample	519.8, 5	503.8, 26	485, 81

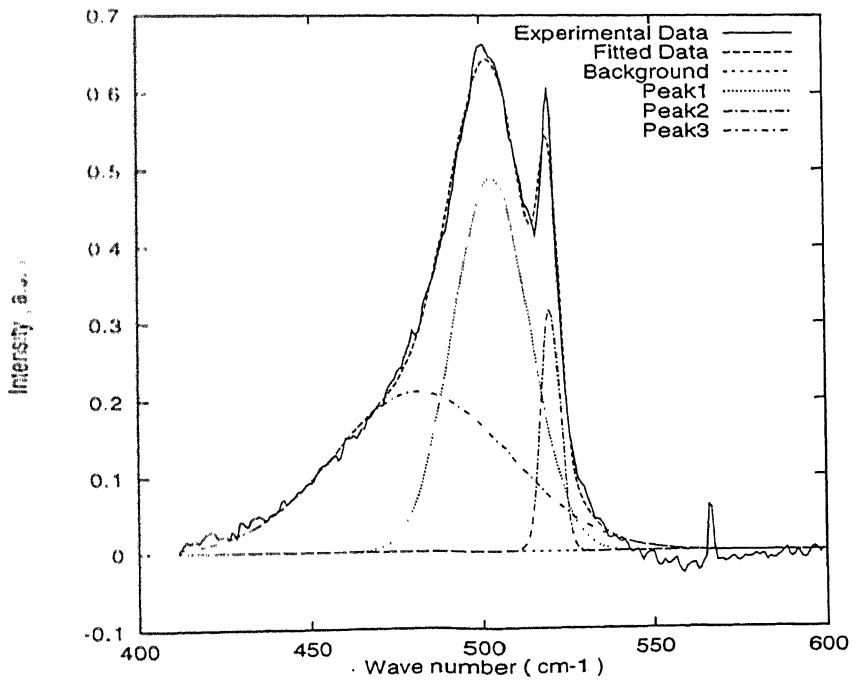
Instead of a simple deconvolution of the spectra, a lineshape analysis including contribution due to disordered phase as well as quantum confinement effect [39] can be carried out. The qualitative conclusions remains unchanged. It may be pointed out that many Raman studies on photoluminescent porous silicon report only on asymmetric red-shifted Si peak (~510 to 520 cm^{-1}) [56]. Non-observation of amorphous silicon phase in such studies can be due to their macro-Raman measurements from a large sample area and small scattering intensities of amorphous silicon phases [57].

Fig. 3.13 shows the effects of heat treatment in vacuum on the same sample. Table 3.2 shows the results of peakfit analysis on these samples. Heating the sample induces structural changes and amorphous content in the sample is increased. Peaks due to nano crystallites shifts to lower frequencies after heat treatment at 495°C and 760°C. This indicates lowering of the crystallite sizes.

One possible mechanism for such structural changes could be the removal of hydrogen and other volatile species from the surfaces of nanocrystallite wires or dots as seen in the thermal effusion spectra. This would leave the crystallites thinner in dimensions. In addition, removal of hydrogen would make the Si surfaces highly reactive. Exposure of these surfaces to air after heat treatment may lead to large oxidation of surfaces. Consequently, the dimensions of silicon skeletons would again be reduced. Indeed, we observe evidence of the oxidation in IR analysis of these samples as shown in the next section. Further, heating at 760°C is probably accompanied



(a)



(b)

Figure 3.13: Raman spectra of porous silicon samples (a) 20 min sample, heated upto 495°C. (b) 20 min sample, heated upto 760°C.

by the collapse of columnar network resulting in a reduction in the intensity from c-Si interface. Increase in disordered silicon content is also supported by the recent observation of high dangling bond density (ESR) and absorption (PDS) on vacuum annealed porous silicon [38].

Raman measurements on samples annealed in air at high temperature (~750°C) show Raman shift similar to the crystalline silicon [39]. These results have been explained in terms of fully oxidized porous silicon and low absorption coefficients of these oxides. Clearly, vacuum annealing is necessary to separate the effects due to structural transformations on heating and oxidation effects.

3.5 IR Analysis

The energy of infrared region of electromagnetic wave spectrum is of the order of vibrational mode energies of various bonds. Therefore, this technique is used to analyze the nature of bonding of Si atoms with hydrogen and oxygen.

We have taken IR transmission spectrum from 600 to 4000 cm^{-1} to look into the vibrational modes in our porous silicon samples. Fig. 3.14 (i) shows the complete spectrum of IR transmission for the following three samples:
(a) 30 min sample, unheated, (b) 20 min sample, unheated, and (c) 20 min sample, heated upto 495°C.

Table 3.3: Assignment of the IR modes observed in electrochemically etched porous silicon

Fig. 3.14 Curve(a)	Fig. 3.14 Curve(b)	Fig. 3.14 Curve(c)	$\omega_{IR}(cm^{-1})$ (Literature [21])	Modes
		3300-3500	3420-3580	O-H stretching
-	-	2240	2250	O-Si-H stretching
2135	2135	-	2030	$Si-H_3$ stretching
2110	2110	-	2110	$Si-H_2$ stretching
2080	2080	-	2070	Si-H stretching
1080	1097	1000-1250	1040-1160	Si-O-Si stretching
895	897	870	870	$Si-H_2$ scissors
845	845	840	835	$Si-H_2$ wagging
650	650	-	640	Si-H bending

Various infrared transmission peaks are listed in Table 3.3 along with their peak assignments from standard literature values.

Following conclusions may be drawn from the infrared transmission data:

1. Peaks due to stretching (~2000-2200 cm^{-1}), bending (650 cm^{-1}), and wagging (845 cm^{-1}) modes of hydrogen are clearly observed. Spectrum in the range of 2000-2400 cm^{-1} are expanded and shown in 3.14 (ii).

2. IR spectra for 20 and 30 minutes anodized samples are similar in nature, except for the expected increase in the hydrogen absorption intensities in thicker sample.

3. Heated sample shows the appearance of new band at ~2240 cm^{-1} (Fig. 3.14(b)), which is assigned to the O-Si-H stretching modes. Silicon hydrides stretching modes are reduced and the sharp structures are disappeared. This is not surprising, and is consistent with our thermal effusion data.

4. There are absorption peaks about 1100 cm^{-1} in as-prepared samples which are assigned to the bulk Si-O-Si asymmetric stretching modes. [8].

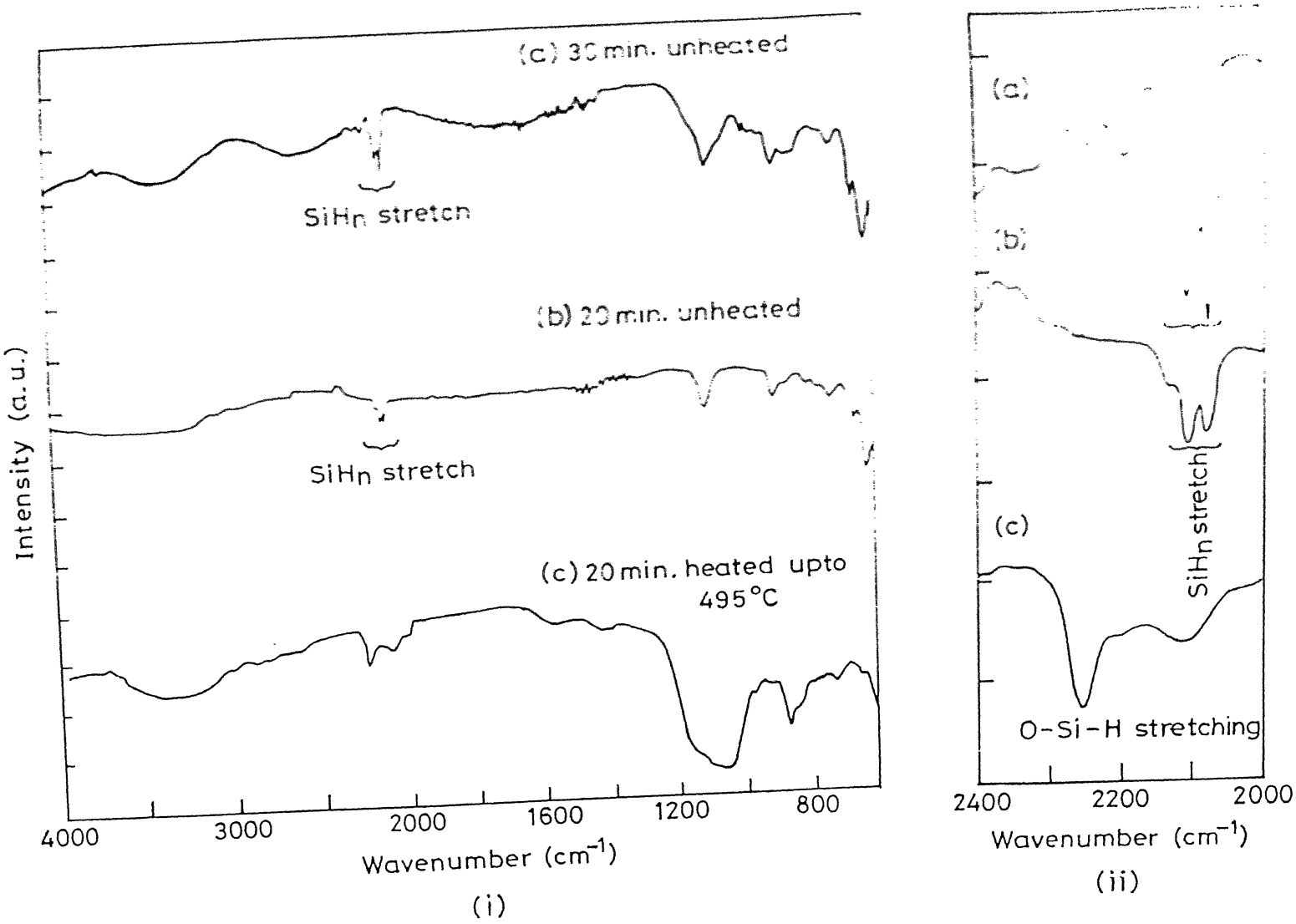


Figure 3.14: IR absorption spectra (a) 20 min sample, unheated (b) 30 min sample, unheated (c) 20 min sample, heated upto 495°C.

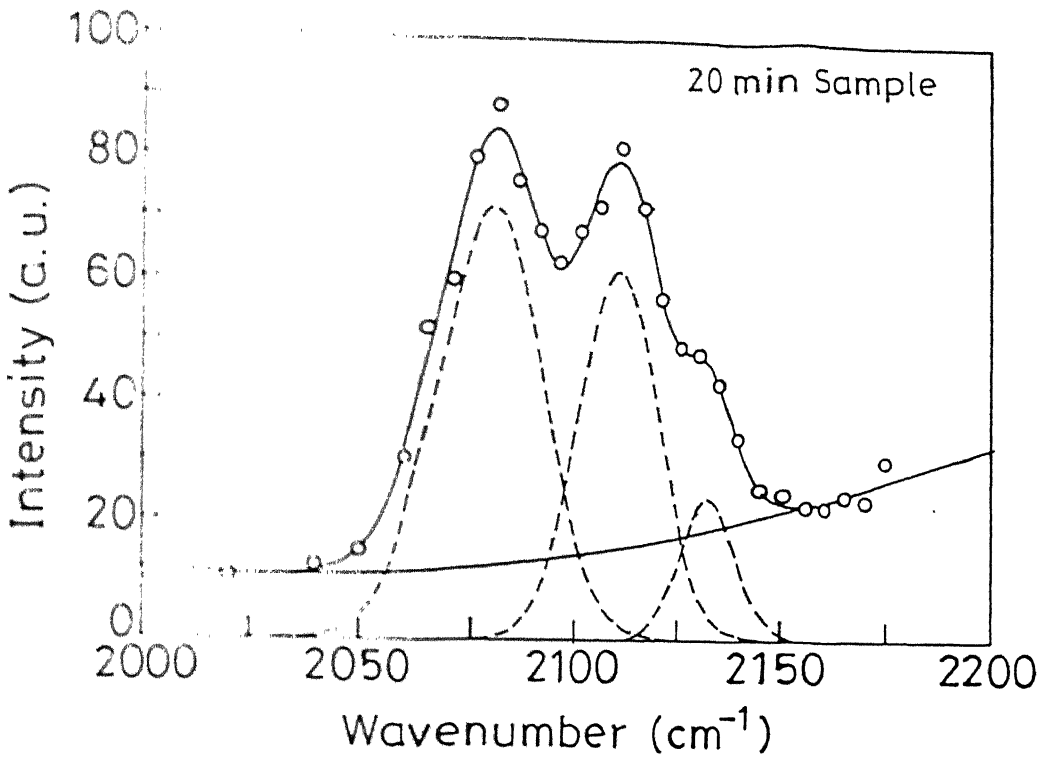


Figure 3.15 Deconvolution of IR spectrum of Fig. 3.14 curve (a) for SiH, SiH_2, and SiH_3 peaks

It is not possible to obtain any quantitative information on the hydrogen content in porous silicon sample due to uncertainties in layer thickness and estimates of PS density. However, relative contributions from mono-, di-, and trihydrides of silicon to the stretching modes can be estimated. Fig. 3.15 shows the deconvolution of corresponding to curve (a) in Fig. 3.14) after background subtractions. Fig. 3.15 shows clearly peaks due to SiH, SiH_2, and SiH_3 are centered at 2080, 2110, and 2133 cm^{-1} respectively. Again their peak widths (FWHM) are 28, 22, and 16 cm^{-1}. These peaks are much sharper and well defined as compared to broad features due to hydrogen in a-Si:H around 2100 cm^{-1}. These results suggest well defined hydrogen chemisorption sites in porous silicon. In view of the large surface to volume ratio ($\sim$200-600 m^2/cm^3) in porous silicon, most of hydrogen is expected to be located at surface sites.

The relative intensities (area) under the stretching modes are found to be 0.53, 0.37 and 0.10 for SiH, SiH_2, and SiH_3, respectively. It is to be noted that the ratio of SiH_2 to SiH comes out to be 2:3 which is similar to that obtained from thermal effusion measurements. These results re-affirm our assignment of LT and HT thermal effusion peaks to SiH_2 and SiH respectively.

Now, it is possible to explain the observation of photoluminescence in our 500°C heated porous silicon sample. As discussed earlier vacuum annealing desorbs hydrogen from the surfaces, increasing the dangling bond densities and reactive sites at the surface. When these surfaces are exposed to air, oxidation occurs (as seen in our IR results). Surface oxides passivate the recombination centers at the surfaces and PL is observed, albeit with lower intensities.

Chapter 4

Summary and Conclusions

The observation of visible photoluminescence in porous silicon has led to considerable effort toward exploitation of its potential use as optoelectronic material. Though there has been many studies on electrical and optical properties of these materials, there is a lack of understanding as regards its thermal stability and influence of various chemical species present in the sample.

In this work, we have prepared porous silicon by the traditional electrochemical etching in HF solution. The thermal stability of the material has been studied by heating the samples in vacuum and mass spectroscopic analysis of species effusing out during the heat treatment. The results have been correlated with infrared and Raman spectroscopic analysis of samples subjected to different heat treatments. The main achievements and conclusions can be summarized as follows:

1. Porous silicon layer of varying thicknesses have been prepared. The samples show bright orange luminescence when viewed with naked eye under UV light at room temperature.

2. Photoluminescence (PL) spectroscopy of these samples show a broad peak at

7. Structural changes on heating in vacuum in porous silicon samples have been observed using Raman spectrum. The size of nano-crystallites decreases and the contribution from disordered component increases from samples heat treated at 495 and 760°C.

8. Infrared spectra of as prepared samples show sharp spectral features around 2100 cm^{-1} due to stretching modes of hydrides of silicon indicating well defined hydrogen chemisorption sites in porous silicon. The porous silicon samples heat treatment at 495°C does not show the infrared peaks due to hydrogen. These sharp features disappear on heating the sample to 495°C consistent with our thermal effusion results. In addition, a broad band around 1000-1200 cm^{-1} corresponding to oxide formation at the surface is observed. The observation of photoluminescence even after heat treatment at 495°C in the sample, has been attributed to the surface passivation of defects due to oxidation.

In summary, room temperature photoluminescent porous silicon samples have been prepared and characterized using a variety of techniques such as infrared, Raman, photoluminescence and thermally stimulated effusion spectroscopy. In particular, thermally stimulated effusion spectra of effusing species have been analyzed in detail to understand the nature of hydrogen bonding and its thermal release from porous silicon. Microstructural information obtained from Raman and infrared spectra have been correlated with the results of thermal effusion studies.

Bibliography

[1] A.Uhlir. *Bell. Syst. Tech. J.*, 35(4):333, 1956.

[2] L.T. Canham. *Appl. Phys. Lett.*, 57:1046, 1990.

[3] A. Halimaoui, C. Oules, G. Bomchil, A. bsiesy, F. Gaspard, R. Harino, M. Ligeon, and F. Muller. *Appl. Phys. Lett.*, 59:304, 1991.

[4] N. Koshida and H. Koyama. *Appl. Phys. Lett.*, 60:347, 1992.

[5] M.A. Tischler, R.T. Collins, J.H. Stathis, and J.C. Tsang. *Appl. Phys. Lett.*, 60:639, 1992.

[6] E. Bassous, M. Freeman, J.-M. Halbout, S.S. Iyer, V.P. Kesan, P. Mungvia, S.F. Pesarcik, and B.L. Williams. *Mater. Res. Soc. Symp. Proc.*, 256:23, 1992.

[7] C. Tsai, K. H. Li, J. Sarathy, S. Shih, and J.C. Campbell. *Appl. Phys. Lett.*, 59(22):2814, 1991.

[8] C. Tsai, K. H. Li, D.S. Kinosky, R. Z. Qian, T. C Hsu, J.T. Irby, and S.K. Banerjee. *Appl. Phys. Lett.*, 60(14):1700, 1992.

[9] J.M. Lavine, S.P. Sawan, Y.T. Shieh, and A.J. Bellezza. *Appl. Phys. Lett.*, 62:1099, 1993.

[10] P. Lim, J.R. Brock, and I. Trachtenberg. *Appl. Phys. Lett.*, 60(4):486, 1992.

[11] N. Koshida and H. Koyama. *Jpn. J. Appl. Phys.*, 30:L1221, 1990.

[12] R. Herino, G. Banchil, K. Barla, C. Bertrand, and J.L. Giroux. *J. Electrochem. Soc.*, 134:1994, 1987.

[13] R.W. Fathauer, T. George, A. Ksondzov, and R.P. Vasquez. *Appl. Phys. Lett.*, 60:995, 1992.

[14] R.E. Hemmel and Sung-Sik Chang. *Appl. Phys. Lett.*, 61(16):1965, 1992.

[15] R.L. Smith and S.D. Collins. *J. Appl. Phys.*, 71:R1, 1992.

[16] George C. John and V.A. Singh. Porous silicon: Theortical studies. *Physics Reports*, 1994.

[17] V. Lehman and U. Gosele. *Appl. Phys. Lett.*, 58:856, 1991.

[18] H. Foll. *Appl. Phys.*, A53:8, 1991.

[19] T. Motohiro, T. Kachi, F. Miura, Y. Takeda, S. Hyoda, and S. Node. *Jpn. J. Appl. Phys.*, 31:L207, 1992.

[20] Y. Hou et. al. *Appl. Phys. Lett.*, 62:1097, 1993.

[21] M.S. Brandt, H.D. Fuchs, M. Stutzmann, J. Webber, and M. Cadona. *Solid State Communication*, 81(4):307, 1992.

[22] Z.Y. Xu, M. Gal, and M. Gross. *Appl. Phys. Lett.*, 60:1375, 1992.

[23] R.P. Vasquez, R.W. Fathauer, T. George, A. Ksendzov, and T.L. Lin. *Appl. Phys. Lett.*, 60:1004, 1992.

[24] T. George, M.S. Anderson, W.T. Pike, L.T. Lin, R.W. Fathuer, K.H. Jung, and D.L. Kwong. *Appl. Phys. Lett.*, 60:2359, 1992.

[25] L.T. Canham, M.R. Houlton, W.Y. Leong, C. Pickering, and J.M. Keen. *J. Appl. Phys.*, 70(1):422, 1991.

[26] T. Maruyama and S. Ohtani. *Appl. Phys. Lett.*, 65(11):1346, 1994.

[27] N. Ookubo, H. Ono, Y.Ochaiai, Y. Mochizuki, and S. Matsui. *Appl. Phys. Lett.*, 61(8):940, 1992.

[28] T. Kimura, A. Yokoi, Y. Nishida, R. Saita, S. Yugo, and T. Ikoma. *Appl. Phys. Lett.*, 67(18):2687, 1995.

[29] Feng Yan, Xi mao Bao, Xias wei Wu, and Hai lan chen. *Appl. Phys. Lett.*, 67(23):3471, 1995.

[30] L. Tsybeskov J. von Behren and P.M. Fauchet. *Appl. Phys. Lett.*, 59(13):1662, 1995.

[31] N.H. Zoubin and M. Vergnat. *Appl. Phys. Lett.*, 65(1):82, 1994.

[32] P. Steiner, F. Kozlowski, and W. Lang. *Appl. Phys. Lett.*, 62:2700, 1993.

[33] Z. Chen and G. Bosman. *Appl. Phys. Lett.*, 62:708, 1993.

[34] F. Namavar, H.P. Maruska, and N.M. Kalphoran. *Appl. Phys. Lett.*, 60:2551, 1992.

[35] P.C. Sercel and D. Kwon. *Appl. Phys. Lett.*, 68(5):684, 1996.

[36] P.M.M.C. Bresses, J.W.J. Knapen, E.A. Meulenkamp, and J.J. Kelly. *Appl. Phys. Lett.*, 61:108, 1992.

[37] N. Hadj Zoubir, M.Vergnat, T. Delatour, A.F. Tasch, J.C. Cambell, B.K. Hance, and J.M. White. *Appl. Phys. Lett.*, 65(1):82, 1994.

[38] L.A. Balagurov, D.G. Yarkin, E.A. Petrova, A.F. Orlov, and S.N. Karyasin. *Appl. Phys. Lett.*, 69:2852, 1996.

[39] A. Roy, K. Jayaram, and A.K. Sood. *Solid State Commun.*, 89:229, 1994.

[40] D.C. Allan, J.D. Joannopolous, and W.B. Poblard. *Phys. Rev. B*, 25:1065, 1982.

[41] W. Beyer and H. Wagner. *J. Appl. Phys.*, 53(12):8745, 1982.

[42] P. Gupta, V.L. Colvin, and S.M. George. *Phys. Rev. B*, 37:8234, 1988.

[43] W. Beyer, H. Wagner, and H. Mell. *Solid State Commun*, 39:375, 1981.

[44] H.E. Kissinger. *Anal. Chem.*, 29:1702, 1957.

[45] Manju Malhotra. *Growth and Structural Characterization of Diamond and Diamondlike Carbon Films*. PhD thesis, I.I.T. Kanpur, 1996.

[46] G. Schulze and M. Henzer. *Surf. Sci.*, 124:336, 1983.

[47] P.A. Readhead. *Vacuum*, 12:203, 1962.

[48] P. Gupta, A.C. Dillion, P.A. Coon, and S.M. George. *Chem. Phys. Lett.*, 176:128, 1991.

[49] A.C. Dillion, P. Gupta, M.B. Robinson, A.S. Bracker, and S.M. George. *J. Electron. Spectrosc. Relat. Phenom.*, 54/55:1085, 1990.

[50] T. George, M.S. Anderson, W.T. Pike, L.T. Lin, R.W. Fathuer, K.H. Jung, and D.L. Kwong. *Appl. Phys. Lett.*, 60:1004, 1992.

[51] N. Islam and S. Kumar. 1994. Unpblished.

[52] M. Thonssen, S. Billat, M. Krüger, H. Lüth, M.G. Berger, U. Frotscher, and U. Rossow. *Appl. Phys. Lett.*, 80:2290, 1996.

[53] Z. Iqbal and S. Veprek. *J. Phys. C: Solid State Phys.*, 15:377, 1982.

[54] S.R. Goodes, T.E. Jenkins, M.I.J. Beale, J.D. Benjamin, and C. Pickering. *Semicond. Sci. Technol.*, 3:483, 1988.

[55] Zhifeng Sui, P.P. Leong, I.P. Herman, and G.S. Higashi. *Appl. Phys. Lett.*, 60(17):2086, 1992.

[56] R. Tsu, H. Shen, and M. Dutta. *Appl. Phys. Lett.*, 60:112, 1992.

[57] J.M. Perez, J. Villalobos, P. Mc Neill, J. Prasad, R. Cheek, J. Kelber, J.P. Estrera, P.D. Steven, and R. Glosser. *Appl. Phys. Lett.*, 61:563, 1992.

123253

Date Slip 123253

This book is to be returned on the date last stamped.